Temporal evolution of single-cell transcriptomes of *Drosophila* olfactory projection neurons

Qijing Xie[1,2], Maria Brbic[3], Felix Horns[4,5], Sai Saroja Kolluru[4], Robert C. Jones[4], Jiefu Li[1], Anay R. Reddy[1], Anthony Xie[1], Sayeh Kohani[1], Zhuoran Li[1], Colleen N. McLaughlin[1], Tongchao Li[1], Chuanyun Xu[1], David Vacek[1], David J. Luginbuhl[1], Jure Leskovec[3], Stephen R. Quake[4,6,7]*, Liqun Luo[1]*, Hongjie Li[1]

[1]Department of Biology, Howard Hughes Medical Institute, Stanford University, Stanford, United States
[2]Neurosciences Graduate Program, Stanford University, Stanford, United States
[3]Department of Computer Science, Stanford University, Stanford, United States
[4]Department of Bioengineering, Stanford University, Stanford, United States
[5]Biophysics Graduate Program, Stanford University, Stanford, United States
[6]Department of Applied Physics, Stanford University, Stanford, United States
[7]Chan Zuckerberg Biohub, Stanford, United States
*For correspondence: steve@quake-lab.org, lluo@stanford.edu

Abstract

Neurons undergo substantial morphological and functional changes during development to form precise synaptic connections and acquire specific physiological properties. What are the underlying transcriptomic bases? Here, we obtained the single-cell transcriptomes of *Drosophila* olfactory projection neurons (PNs) at four developmental stages. We decoded the identity of 21 transcriptomic clusters corresponding to 20 PN types and developed methods to match transcriptomic clusters representing the same PN type across development. We discovered that PN transcriptomes reflect unique biological processes unfolding at each stage—neurite growth and pruning during metamorphosis at an early pupal stage; peaked transcriptomic diversity during olfactory circuit assembly at mid-pupal stages; and neuronal signaling in adults. At early developmental stages, PN types with adjacent birth order share similar transcriptomes. Together, our work reveals principles of cellular diversity during brain development and provides a resource for future studies of neural development in PNs and other neuronal types.

Introduction

Cell-type diversity and connection specificity between neurons are the basis of information processing underlying all nervous system functions. The precise assembly of neural circuits involves multiple highly regulated steps. First, neurons are born from their progenitors and acquire unique fates through a combination of (1) intrinsic mechanisms, such as lineage, birth order, and birth timing; (2) extrinsic mechanisms, such as lateral inhibition and extracellular induction, and (3) developmental stochasticity in some cases (Jan & Jan, 1994; Johnston & Desplan, 2010; Kohwi & Doe, 2013; Holguera & Desplan, 2018; Li et al., 2018). During wiring, neurons extend their neurites to a coarse targeting region, elaborate their terminal structures, select pre- and post-synaptic partners, and finally form synaptic connections (Sanes & Yamagata,

2009; Jan & Jan, 2010; Kolodkin & Tessier-Lavigne, 2011; Luo, 2020; Sanes & Zipursky, 2020). Studies from the past few decades have uncovered many molecules and mechanisms that regulate each of these developmental processes.

The development of *Drosophila* olfactory projection neurons (PNs) has been extensively studied (Jefferis et al., 2004; Hong & Luo, 2014). PNs are the second-order olfactory neurons that receive organized input from olfactory receptor neurons (ORNs) at ~50 stereotyped and individually identifiable glomeruli in the antennal lobe, and carry olfactory information to higher brain centers (Vosshall & Stocker, 2007; Wilson, 2013) (**Figure 1A**). Different types of PNs send their dendrites to a single glomerulus or multiple glomeruli (Marin et al., 2002; Lai et al., 2008; Yu et al., 2010; Tanaka et al., 2012; Bates et al., 2020). PNs are derived from three separate neuroblast lineages—anterodorsal, lateral, and ventral lineages, corresponding to their cell bodies' positions relative to the antennal lobe (Jefferis et al., 2001). PNs produced from the anterodorsal and lateral lineages (adPNs and lPNs) are cholinergic excitatory neurons. The fate of uniglomerular excitatory PN types, defined by their glomerular targets, is predetermined by their lineage and birth order (Jefferis et al., 2001; Marin et al., 2005; Yu et al., 2010; Lin et al., 2012). PNs produced from the ventral lineage (vPNs), on the other hand, are GABAergic inhibitory neurons (Jefferis et al., 2007; Liang et al., 2013; Parnas et al., 2013). The connectivity and physiology of PNs have also been systematically studied (Bhandawat et al., 2007; Jeanne et al., 2018; Bates et al., 2020).

Despite the fact that PNs are among the most well-characterized cell types in all nervous systems, their transcriptome-wide gene expression changes across different developmental stages with cell-type specificity are still unknown. This information can help us obtain a more complete picture of both known and unexplored pathways underlying neural development and function. Recently, the advent of single-cell RNA sequencing (scRNA-seq) has paved the way towards obtaining such data (Li et al., 2017; Kalish et al., 2018; Zhong et al., 2018; Li, 2020). Here, we profiled and analyzed the single-cell transcriptomes of most uniglomerular excitatory PNs. We identified the correspondence between two-thirds of transcriptomes and PN types at one stage and developed methods to reliably match transcriptomic clusters corresponding to the same types of PNs across different stages. We discovered that PN transcriptomes exhibit unique characteristics at different stages, including birth-order, neurite pruning, wiring specificity, and neuronal signaling. The identification of many differentially expressed genes among different PN types, such as transcription factors, cell-surface molecules, ion channels, and neurotransmitter receptors, provides a rich resource for further investigations of the development and function of the olfactory system.

Results

Single-cell transcriptomic profiling of *Drosophila* PNs at four developmental stages

The development of PNs follows the coordinated steps as previously described (Hong & Luo, 2014). 18 out of 40 types of adPNs are born embryonically and participate in the larval olfactory system. Then, during the larval stage, the rest of adPNs and all lPNs are born (Jefferis et al., 2001; Marin et al., 2005; Yu et al., 2010; Lin et al., 2012). During early metamorphosis following puparium formation, embryonically born PNs first prune terminal branches of dendrites and axons, and then re-extend their dendrites into the future adult antennal lobe, and axons into the mushroom body and lateral horn following the neurites of larval-born PNs (Marin

et al., 2005). From 0 to 24 hours after puparium formation (APF), PNs extend their dendrites into the developing antennal lobe and occupy restricted regions. ORN axons begin to invade antennal lobe at ~24 hours APF. PN dendrites and ORN axons then match with their respective partners beginning at ~30 hours APF and establish discrete glomerular compartments at ~48 hours APF. Thereafter, they expand their terminal branches, build synaptic connections, and finally form mature adult olfactory circuits (Jefferis et al., 2004) (**Figure 1B**).

To better understand the molecular mechanisms that control these dynamic developmental processes underlying neural circuit assembly, we performed scRNA-seq of PNs from 4 different developmental stages: 0–6 hours APF, 24–30 hours APF, 48–54 hours APF, and 1–5 days adult (hereafter 0, 24, 48h APF and adult) (**Figure 1C**). We used *GH146-GAL4* (Stocker et al., 1997) to drive *UAS-mCD8-GFP* (Lee & Luo, 1999) expression in most PNs at 24h, 48h, and adult, which labels ~90 of the estimated 150 PNs in each hemisphere, covering ~40 of the 50 PN types. At 0h APF, *GH146-GAL4* also labels cells in the optic lobes (**Figure 1—figure supplement 1A**), which are inseparable from the central brain by dissection. Therefore, we used *VT033006-GAL4* to label PNs at 0h APF (**Figure 1C** and **Figure 1—figure supplement 1B**) (Tirian & Dickson, 2017). *VT033006-GAL4* labels most PNs from the anterodrosal and lateral lineage, but not PNs from the ventral lineage or anterior paired lateral (APL) neurons like *GH146-GAL4*. It is expressed in ~95 cells that innervate ~44 glomeruli which largely overlap with PNs labeled by *GH146-GAL4* (Inada et al., 2017; Elkahlah et al., 2020). In addition to PNs labeled by *GH146-GAL4* and *VT033006-GAL4* (we will refer to them as 'most PNs' hereafter), we have collected single-cell transcriptomic data using drivers that only label a small number of PN types for mapping the transcriptomic clusters to anatomically defined PN types.

For scRNA-seq, fly brains with a unique set of PN types labeled using different drivers at each developmental stage were dissected and dissociated into single-cell suspensions. GFP+ cells were sorted into 384-well plates by fluorescence-activated cell sorting (FACS), and sequenced using SMART-seq2 (Picelli et al., 2014) (**Figure 1D**) to a depth of ~1 million reads per cell (**Figure 1—figure supplement 1C**). On average ~3000 genes were detected per cell (**Figure 1—figure supplement 1D**), and after quality filtering (see Methods), we obtained ~3700 high quality PNs in addition to the previously sequenced ~1200 PNs (Li et al., 2017) , yielding ~4900 PNs for analysis in this study (**Figure 1E**). All analyzed PNs express high levels of neuronal markers but not glial markers, confirming the specificity of sequenced cells (**Figure 1—figure supplement 1E**). Unbiased clustering using overdispersed genes from all PNs readily separates them into different groups according to their stage (**Figure 1F**), suggesting that gene expression changes across these four developmental stages represent a principal difference in their single-cell transcriptomes.

Decoding the glomerular identity of transcriptomic clusters by sequencing subsets of PNs at 24h APF

PNs labeled by *GH146-GAL4* at 24h APF form ~30 distinct transcriptomic clusters. We previously matched 6 of these transcriptomic clusters to specific anatomically and functionally defined PN types (Li et al., 2017) , hereafter referred to as "decoding transcriptomic identity." Unlike ORNs, whose identities can be decoded using uniquely expressed olfactory receptors (Li et al., 2020a), PNs lack known type-specific markers. Instead, PN types are mostly specified by combinatorial expression of several genes (Li et al., 2017), making it more challenging to decode their transcriptomic identities.

To circumvent these challenges and decode the transcriptomic identities of more types of PNs, we took advantage of the extensive driver line collection in *Drosophila* (Luan et al., 2006; Jenett et al., 2012; Dionne et al., 2018). We searched for split-GAL4 lines that only labeled a small proportion of all PNs (Yoshi Aso, unpublished data). Using such drivers, we could sequence a few types of PNs at a time, plot those cells with most PNs, and then use differentially expressed markers among them to decode their identities one-by-one.

split#28-GAL4 labeled two types of PNs—those that project their dendrites to the DC3 and DA4l glomeruli in developing and adult animals (**Figure 2A, B**; note that PN types are named after the glomeruli they project their dendrites to). We sequenced those PNs (*split#28+* PNs hereafter) at 24h APF. We chose this stage because this is when different PN types exhibit the highest transcriptome diversity as hinted by the number of clusters seen in Figure 1F (see following sections for more detailed analysis). To visualize sequenced *split#28+* PNs, we performed dimensionality reduction using 561 genes identified from most 24h PNs using Iterative Clustering for Identifying Markers (ICIM), an unsupervised machine learning algorithm (Li et al., 2017), followed by embedding in the tSNE space. *Split#28+* PNs (orange dots) fell into two distinct clusters and intermingled with *GH146+* PNs (grey dots) (**Figure 2C**). One cluster mapped to previously decoded DC3 PNs (Li et al., 2017), and the other cluster expressed *zfh2* (**Figure 2—figure supplement 1A**). We validated that this cluster indeed represents DA4l PNs by visualizing the expression of *zfh2* in PNs utilizing an intersectional strategy by combining *zfh2-GAL4, GH146-Flp,* and *UAS-FRT-STOP-FRT-mCD8-GFP* (hereafter referred to as "intersecting with *GH146-Flp*") (**Figure 2—figure supplement 1B**).

split#7-GAL4 labeled 3 types of PNs in the adult stage (**Figure 2—figure supplement 2A**). However, when we sequenced cells labeled by this GAL4 line at 24h APF and visualized them using tSNE, we found 8 distinct clusters (**Figure 2F**). We reasoned that this could be due to loss of driver expression in adult stage for some PN types. To test this hypothesis and reveal PNs that are labeled by this driver transiently during development, we used a permanent labeling strategy to label all cells that express *split#7-GAL4* at any time of development (*split#7+* PNs hereafter) by combining it with *UAS-mCD8-GFP*, *Actin promoter-FRT-STOP-FRT-GAL4*, and *UAS-Flp.* Using this strategy, we observed labeling of 8 types of PNs (**Figure 2D**), consistent with number of clusters we observed by sequencing. Among *split#7+* PNs, 4 types belong to the adPN lineage (*acj6+*) and the other 4 types belong to the lPN lineage (*vvl+*) (**Figure 2E**). Only 1 lPN type, DA1 (*CG31676+*), has previously been decoded (**Figure 2—figure supplement 2B**). We identified differentially expressed genes among *split#7+* PNs and obtained existing GAL4 lines mimicking their expression. By intersecting those GAL4 lines with *GH146-Flp,* we mapped all 7 previously unknown transcriptomic clusters to 7 PN types (**Figure 2—figure supplement 2 C–H**; see legends for detailed description).

In addition to screening through collections of existing driver lines, we also utilized scRNA-seq data to find drivers that label a subpopulation of PNs. One such marker was the gene *knot (kn),* which was expressed in 7 transcriptomic clusters among all *GH146+* PNs (**Figure 2—figure supplement 3A**). One of the *kn+* clusters expressing *trol* has been previously mapped to VM2 PNs (Li et al., 2017). When *kn-GAL4* was intersected with *GH146-Flp,* 6 types of adPNs (*acj6+*) and several vPNs (*Lim1+*) were labeled (**Figure 2G, J**). Among the 6 adPN types, VM7 and VM5v PNs were also labeled by *split#15-GAL4* (**Figure 2H**). Although it has been previously reported that *GH146-GAL4* is not expressed in VM5v PNs (Yu et al., 2010), labeling of these PNs when *GH146-Flp* was intersected with either *kn-GAL4* or *split#15-GAL4* indicates

that *GH146-Flp* must be expressed in VM5v PNs at some point during development. Using *split#15-GAL4*, we were able to decode the two clusters to be either VM7 or VM5v PNs (**Figure 2—figure supplement 3B**). Due to the lack of existing GAL4 drivers for differentially expressed genes between these two clusters, we could not further distinguish them so far; their identities can be decoded by creating new GAL4 drivers in future studies. Other than these two clusters, we were able to match transcriptomic clusters and glomerular types for the rest of *kn+* adPNs one-to-one (**Figure 2—figure supplement 3C–E**). In addition to excitatory PNs, one *kn+* vPN type innervated DA1 glomerulus (because DA1 glomerulus is innervated only by lPNs and vPNs, not adPNs). We found that *DIP-beta* was expressed in one *kn+* vPN cluster but not in lPNs innervating DA1 glomerulus (**Figure 2—figure supplement 3F, G**). Intersecting *DIP-beta-GAL4* with *GH146-Flp* confirmed that *DIP-beta+* vPN indeed targeted their dendrites to DA1 glomerulus, illustrating the *DIP-beta+* vPN cluster to be DA1 vPNs (**Figure 2—figure supplement 3H**).

In summary, by sequencing a small number of known PN types at a time and analyzing the expression pattern of differentially expressed genes, we have now mapped a total of 21 transcriptomic clusters corresponding to anatomically defined PN types at 24h APF (**Figure 2K, L**). Ultimately, we aimed to match the transcriptomes of the same PN types across development. As an intermediate step, we carried out global analysis of gene expression changes across development, which could help us reliably identify transcriptomic clusters representing different PN types at different developmental stages.

Global gene expression dynamics across four developmental stages

All sequenced PNs segregated into different clusters according to their developmental stages using unbiased, over-dispersed genes for clustering regardless of PN types (**Figure 1F**). Even when we used the genes identified by ICIM for clustering, which emphasizes the differences between different PN types (Li et al., 2017), we still observed that individual PNs were separated principally by developmental stages (**Figure 3A**). Together, these observations illustrate global transcriptome changes of PNs from pupa to adult.

To understand what types of genes drive this separation, we searched for genes that were differentially expressed in different developmental stages (**Figure 3B, C**). We clustered the genes into different groups based on their expression pattern throughout development. Seven groups of genes showed clear developmental trends—five groups were down-regulated from pupa to adult and two groups were up-regulated (**Figure 3D, E**). Consistent with our previous knowledge, neural development-related genes, including those with functions in morphogenesis and cytoskeleton organization, were enriched in developing PNs (**Figure C, D**); genes related to synaptic transmission, ion transport, and behavior, on the other hand, were up-regulated in mature PNs (**Figure C, E**) (Li et al., 2017; Li et al., 2020b).

Single-cell transcriptomes of PNs reveal dominant biological processes at different stages of development

Because PN transcriptomes exhibited global development-dependent dynamics, we needed to find a method to reliably and consistently classify transcriptomic clusters representing different PN types at all stages. We first identified informative genes for clustering from each stage using ICIM and used them for further dimensionality reduction. However, using this method, we obtained different numbers of clusters at each stage (**Figure 4A**). Closer examination of each stage revealed unique biological features of PN development.

At 0h APF, PNs always formed two distinct clusters—a larger cluster consisting of both adPNs and lPNs, and a smaller one with only adPNs (**Figure 4B**, **Figure 4—supplement 2A**). As introduced earlier, although all lPNs and many adPNs are born during the larval stage, some adPNs are born during the embryonic stage. We hypothesized that the smaller cluster could represent embryonically born PNs, which undergo axon and dendrite pruning during early metamorphosis (Marin et al., 2005). Neurite pruning in *Drosophila* depends on cell autonomous action (Lee et al., 2000) of the steroid hormone ecdysone receptor (EcR) (Levine et al., 1995; Thummel, 1996; Schubiger et al., 1998; Lee et al., 2000). Upon binding of the steroid hormone ecdysone, EcR and its co-receptor Ultraspiracle (Usp) form a complex to activate a series of downstream targets, including a transcription factor called Sox14, which in turn promotes expression of the cytoskeletal regulator Mical and Cullin1 SCF E3 ligase (**Figure 4C**) (Lee et al., 2000; Kirilly et al., 2009; Kirilly et al., 2011; Wong et al., 2013). To test our hypothesis, we examined the expression of genes which are known to participate in neurite pruning and genes that showed elevated expression in the mushroom body γ neurons during pruning (Alyagor et al., 2018). We found that *Sox14*, *Mical*, *Cullin1*, and two sorting complexes required for transport (ESCRT) genes—*shrb* and *Vps20*, indeed showed higher expression levels in the smaller cluster (**Figure 4D**). We also confirmed our hypothesis by mapping two types of embryonically born PNs, DA4l and VA6 PNs, to this smaller cluster (**Figure 4—figure supplement 2B**; see mapping details in Figure 7).

At 24h APF, we observed the highest number of clusters reflecting different PN types. Moreover, dimensionality reduction using the top 2000 overdispersed genes also showed more distinct clusters at this timepoint compared to the others (**Figure 4—figure supplement 1**). Quantifications of transcriptomic similarity among PNs at each stage indeed confirmed the highest diversity among PNs at 24h APF (**Figure 4E–G**). This is likely explained by the fact that at this stage, PNs refine their dendrites to specific regions and begin to prepare themselves as targets for their partner ORN axons. In addition, PN axons at the lateral horn begin to establish their characteristic branching patterns (Jefferis et al., 2004). All these processes require high level of molecular diversity among different PN types to ensure precise wiring, warranting more distinction between their transcriptomes at this stage.

In contrast to the high transcriptomic diversity in 24h APF PNs, adult PNs only formed three clusters (**Figure 4A** bottom, indicated by dashed lines). The three clusters represent cholinergic excitatory PNs (marked by *VAChT*), and two *Gad1+* GABAergic inhibitory cell types—vPNs and APL neurons (*VGlut+*), respectively (**Figure 4H**). This is likely because after wiring specificity is achieved, all excitatory PNs may perform similar functions, but distinct from inhibitory neuronal types.

Thus, at different developmental stages, the differentially expressed genes we identified all revealed the most defining biological processes those neurons are undertaking. Our observations showed that PN transcriptomes reflect the pruning process of embryonically born PNs at 0h APF, PN type and wiring distinction at 24h APF, and neurotransmitter type in adults.

Identifying PN types at all developmental stages

With the exception of the 24h APF PNs, gene sets identified from each of the other stages could not resolve distinct clusters reflecting PN type diversity (**Figure 4**). Therefore, we tried to use the genes identified by ICIM from 24h APF PNs to cluster PNs of the other stages. We found that this gene set outperformed all other gene sets in separating different PN types at all

timepoints (**Figure 5A**). In fact, most gene sets found by different methods at 24h APF, including overdispersed genes, ICIM genes, as well as differentially expressed genes between different clusters, exceeded gene sets identified at other stages for clustering PNs according to their types (data not shown), further confirming that transcriptomes of 24h APF PNs carry the most information for distinguishing different PN types, even for other developmental stages.

Following this observation, we decided to use differentially expressed genes between 24h PN clusters for PN-type identification for all stages. We applied meta-learned representations for single cell data (MARS) for identifying and annotating cell types (Brbic et al., 2020). MARS learns to project cells using deep neural networks in the latent low-dimensional space in which cells group according to their cell types. We used 24h APF, the stage with highest transcriptome diversity, as the starting annotated dataset to learn shared low-dimensional space for 48h APF, 0h APF, and eventually the adult dataset. Using this approach, we found ~30 cell types in each stage (**Figure 5B**). Independently, we also validated MARS cluster annotations using two distinct methods: HDBSCAN clustering based on tSNEs or Leiden clustering based on neighborhood graphs (**Figure 5—figure supplement 1**) (Blondel et al., 2008; Levine et al., 2015; Traag et al., 2019). Clusters identified by HDBSCAN and Leiden largely agreed with MARS annotations, confirming the reliability of MARS. We compared cluster annotations by these three methods to known PN types at 24h APF (**Figure 5—figure supplement 1C**) and found that even at this stage, MARS performed better at segregating some closely related clusters representing multiple PN types (**Figure 5—figure supplement 1D**). At 0h APF and the adult stage, MARS identified more clusters compared to the other methods, demonstrating the robustness of MARS at identifying unique cell types.

Matching the same PN types across four developmental stages

We next sought to match transcriptomes of the same PN type across different developmental stages. We first tried to apply some batch correction methods, including Harmony, BBKNN, combat, and Scanorama, to our dataset to correct for the transcriptomic changes of PNs throughout development (Hie et al., 2019; Korsunsky et al., 2019; Polanski et al., 2020). For all batch methods attempted, we observed instances of (1) PNs of the same type at the same stage split into different clusters; (2) PNs of different types merge into the same cluster; (3) no distinguishable cluster formation for many PNs in stages other than 24h APF. Therefore, we needed to develop alternative approaches to reliably match transcriptomes of same PN types across different developmental stages. To perform this task, we first used *kn+* PNs as test case. We collected PNs labeled by *kn-GAL4* from 24h APF, 48h APF, and adult brains for scRNA-seq (**Figure 6A**). Dimensionality reduction of these cells showed a consistent number of clusters across stages (**Figure 6B**). One exception is an extra vPN cluster observed at 48h APF and adult stages. This discrepancy with 24h APF data is likely caused by the lower number of vPNs sequenced at 24h APF.

When *kn+* PNs from all three stages were plotted together, all adPNs (*acj6+* clusters on the upper side) formed relatively distinct clusters and did not intermingle with adPNs from the other timepoints (**Figure 6C**), reflecting substantial changes in the transcriptome of the same type of PNs across development. To match the same type of PNs, we took two independent approaches (**Figure 6D**). In the first approach, clusters were automatically matched based on their transcriptomic similarity. Briefly, we identified a set of genes that were differentially expressed in each cluster compared to all the rest at the same stage. Then, we calculated the percentage of genes shared between each pair of clusters across two stages (Jaccard similarity

index) (**Figure 6E**). If two clusters from two stages both had the highest similarity score with each other, we considered them to be matched. In the second approach, we used markers that were expressed in a consistent number of clusters at each stage. Those markers, or marker combinations, were used to manually match the same type of PNs (some example markers used are shown in **Figure 6F**). Using these two approaches, we were able to match the same types of PNs across three developmental stages, and the results from the two approaches consistently agreed with each other (**Figure 6G**). In addition, these data further validated an earlier conclusion (**Figure 4**) that as development proceeds from 24h APF and 48h APF to adults, the transcriptomic difference between identified PN types becomes smaller (**Figure 6G**; quantified in **Figure 6—figure supplement 1**).

We next applied the same approaches for matching *kn+* PN types across 3 stages to match most PNs (sequenced using either *GH146-GAL4* or *VT033006-GAL4*) across 4 stages (**Figure 7A**). In addition to marker gene expression, we also used subset of PNs we had sequenced from different stages to manually match PN types (**Figure 7—figure supplements 1A–D**). For the manually matched PN types with known identity, we summarized markers and marker combinations we used in a dot plot, where both average expression as well as percentage of cells expressing each marker were shown (**Figure 7—figure supplement 2**). Using both manual and automatic approaches, we were able to match many PN types across 2 or more developmental stages (**Figure 7B**), which includes 18 PN types that we have decoded in **Figure 2** and 7 transcriptomic clusters with unknown identity. The majority of the PNs we matched were confirmed by both the automatic (transcriptomic similarity-based) and manual (marker-based) methods (**Figure 7C** and **Figure 7—figure supplement 1E**).

PN types with adjacent birth order share more similar transcriptomes at early stages of development

Previous works have shown that the PN glomerular types are prespecified by the neuroblast lineages and birth order within each lineage (Jefferis et al., 2001; Marin et al., 2005; Yu et al., 2010; Lin et al., 2012) (**Figure 8A**). Having decoded the transcriptomic identities of different PN types at different timepoints, we can now ask the extent to which transcriptomic similarity is contributed by lineage and birth order, and whether these contributions persist through development.

To address these questions, we performed hierarchical clustering on all excitatory PN clusters we identified from each timepoint. We plotted the dendrogram and the correlation between each pair of clusters (**Figure 8—figure supplement 1**). We observed some lineage-related similarity between PN types at 0h APF: transcriptomes of PNs from the same lineage tended to be clustered together in the dendrogram and their correlations are higher, although the relationship was not absolute. Such similarity was gradually lost as development proceeded (as inferred by both the dendrogram as well as correlation between PNs from the same lineage). Interestingly, we noticed that some PNs with adjacent birth order appeared to be neighbors in the dendrogram at 0h and 24h APF.

To further investigate the relationship between birth order of PNs and their transcriptomic similarity, we selected all decoded PNs from the anterodorsal lineage, ordered them according to their birth order, and computed their correlation (**Figure 8B**). 0h APF adPNs showed high correlation between their birth order and their transcriptomic similarity, as indicated by the high correlations in boxes just off the diagonal line. To test if the transcriptomic similarity of adPNs

indeed covaries with their birth order, we performed permutation tests, comparing the Spearman correlations between birth-order ranking and transcriptomic similarity ranking (**Figure 8C**, see Materials and Methods for details). The results confirmed that 0h and 24h APF PNs, but not 48h APF and adult PNs, exhibited high correlations between their birth orders and transcriptomic similarities. In addition, developmental trajectory analysis of adPNs born at the larval stage using Monocle 3 (Cao et al., 2019) also showed that the unbiased pseudo time recapitulated their birth order (**Figure 8D**).

A previous study profiled the transcriptomes of PN neuroblasts at various larval stages and identified 63 genes with temporal gradients (Liu et al., 2015). Among those genes, the authors have validated that two RNA-binding proteins, Imp and Syp, regulate the fate of PNs born at different times. Therefore, we analyzed expression of these 63 genes at 0h APF to see if any of these genes with temporal gradients has persisted expression in postmitotic PNs. We found 15 out of the 63 genes (including *Imp* but not *Syp*) maintained some temporal gradient patterns according to their birth order at 0h APF (**Figure 8E**) but not at the later stages (data not shown). This result suggested that the expression of a subset of birth order-related genes in adPN neuroblast, including a cell-fate regulator, is maintained in postmitotic PNs till early pupal stage.

In summary, our data demonstrated that PN types with adjacent birth order shared more similar transcriptomes, reflecting temporal gene expression dynamics of their progenitor. Such transcriptomic similarity was maintained at early pupal stages and was gradually lost as PNs mature.

Differentially expressed genes in different PN types

Hierarchical clustering on the principal components calculated using the entire gene matrix indicates that the similarities between different PN types are not fixed across development (**Figure 8—figure supplement 1**). This suggests that the differentially expressed genes in PNs differ across developmental stages. Identifying differentially expressed (DE) genes, especially among those that we have matched across multiple developmental stages (**Figure 7**), can allow us to investigate expression dynamics in different PN types and also reveal interesting molecules for future studies.

We consider a gene to be differentially expressed if it has an adjusted p-value of less than 0.01 by Mann-Whitney U test in at least one cluster compared to the rest of the clusters. Using this criterion, we found around 500 DE genes at 24h APF, 48h APF, and the adult stage (**Figure 9A**). At 0h APF, many more DE genes were identified. The larger gene set at this stage is mostly contributed by the embryonically born PNs (1015 out of 1393 genes), which have transcriptomically distinct features because these neurons undergo axon and dendrite pruning (**Figure 4A–D)**. We intersected the four lists of DE genes to find genes that are differentially expressed throughout development. This resulted in 103 genes, 52 of which were differentially expressed among the 12 PN types we matched across all four stages. Among the DE genes that are differentially expressed in all four stages, we observed an over-representation of transcription factors (TFs) and cell surface molecules (CSMs) compared to their genome-wide fractions (**Figure 9B**). Previous studies have shown that genes in these two categories play critical roles in PN wiring (Hong & Luo, 2014; Li et al., 2017). We therefore further explored the expression pattern of these genes (**Figure 9C** and **Figure 9—figure supplements 1 and 2**).

While the majority of TFs are expressed in both lineages, expression of a small fraction of TFs is lineage-specific. For example, expression of *acj6*, *kn*, *C15*, and *salr* is limited to PNs

from the anterodorsal lineage, whereas *vvl* and *unpg* are only expressed in PNs from the lateral lineage (**Figure 9C** and **Figure 9—figure supplement 1**). Furthermore, whereas TFs are generally expressed in a binary fashion throughout development (**Figure 9C** and **Figure 9—figure supplement 1**), many CSMs exhibit graded expression with complex temporal dynamics (**Figure 9D** and **Figure 9—figure supplement 2**). This is consistent with observations made from single-cell transcriptome studies in the developing *Drosophila* optic lobe (Kurmangaliyev et al., 2020; Ozel et al., 2020). Among the CSMs that are differentially expressed in any of the 4 stages, we observed many molecules in protein families that have been implicated in wiring, including Beaten Path (Beat), Dpr, DIP, Dscam, Fasciclin (Fas), and Robo (**Figure 9—figure supplement 2**) (Kolodkin & Tessier-Lavigne, 2011; Sanes & Zipursky, 2020). Thus, this differentially expressed gene list may contain an enriched set of wiring-related molecules, some of which have been studied in the context of wiring. Therefore, our data can serve as a useful resource for future studies of wiring specificity. On the other hand, we note that some genes with differential expression pattern at the protein level, such as Ten-a and Ten-m (Hong et al., 2012), do not exhibit obvious differential expression at the mRNA level. This highlighted the existence of post-transcriptional regulation for some genes that are not captured by transcriptomic analysis.

Genes involved in metabolism and neuronal signaling are differentially expressed among adult PNs

Our analyses have shown that transcriptomic differences between different PN types diminish as development proceeds (**Figure 4**). However, different PN types in adults still exhibited differential gene expression (**Figure 9**). Such differential expression could be contributed by residual developmentally differentially expressed genes, by new categories of differentially expressed genes in mature PNs reflecting functional differences between different PN types, or a combination of both. To distinguish between these possibilities, we compared DE genes among different transcriptomic clusters of PNs at 24h APF and at the adult stage.

We found that more than a third of the DE genes were shared between these two stages (**Figure 10A**). Gene ontology analysis revealed that these shared genes were predominately related to neural development (**Figure 10B**, middle). These data suggested that some DE genes found among adult PN types were developmentally differentially expressed genes, some of which could play a role in the maintenance of adult nervous system structures.

Interestingly, many gene ontology terms related to the physiological properties of PNs were observed among the adult-only DE genes (**Figure 10B**, bottom). In addition, we observed several ion-channels and neurotransmitter receptors in the list of CSMs with differential expression pattern (**Figure 9—figure supplement 2**). Indeed, several adult DE genes belong to the ion channels or transmembrane receptor (including neurotransmitter receptors and G-protein-coupled receptors) gene groups (**Figure 10C**). These results demonstrated that PN types in adults acquire new categories of differentially expressed genes, and those genes might lead to differences in the physiological properties between different PN types.

Discussion

Deciphering single-cell transcriptomes for connectivity-defined neuronal types

Traditionally, neurons are classified based on their morphology, physiology, connectivity, and signature molecular markers. More recently, scRNA-seq has allowed classification of cell types

based entirely on their transcriptomes. Many studies have illustrated that cell-type classification based on the single-cell transcriptomes largely agrees with classifications by some of the more traditional criteria (Zeng & Sanes, 2017).

For *Drosophila* olfactory PNs, the most prominent type-specific feature is their pre- and post-synaptic connections, which determines their olfactory response profiles and the higher order neurons they relay olfactory information to. Thus, different PN types are largely defined by the differences in their connectivity. We have previously observed that the transcriptomic identity of PNs corresponds well with their types during development, and for three identified PN types, transcriptomic differences peak during the circuit assembly stage (Li et al., 2017). Here, we generalized these findings across many more PN types by showing that transcriptomic differences are the highest around 24h APF, a stage when PNs are making wiring decisions and preparing cues for subsequent ORN–PN matching (**Figure 4**), and by demonstrating that clustering of PNs according to their types from all stages are best done using differentially expressed genes at 24h APF (**Figure 5**). Additionally, our data indicate that at certain stages, differences among those type-specific genes can be masked by other genes belonging to pathways of a more dominating biological process (such as neurite pruning at 0h APF for PNs). As a consequence, it may be challenging to identify genes carrying type-specific information at certain timepoints even when sophisticated algorithms are applied, which can lead to underestimation of cell type diversity. Our observation of peaked transcriptome diversity in developing projection neurons has also been observed in the *Drosophila* optic lobe recently (Ozel et al., 2020). Thus, in order to accurately classify single-cell transcriptomes, especially for connectivity-defined neuronal types such as fly olfactory PNs, it may be a general strategy to first obtain their single-cell transcriptomes during circuit assembly and then use this information to supervise cell-type classification in other developmental stages, including adults.

Tracing the same cell type in different states

Both cell types and their biological states can split single-cell transcriptomes into distinct clusters (Zeng & Sanes, 2017; Cembrowski & Menon, 2018; Tasic, 2018). We observed that the same PN types of different developmental stages—reflecting different states—indeed exhibit very distinct transcriptomic profiles (**Figures 5**, **6**). To identify transcriptomic clusters corresponding to the same PN types across multiple timepoints, we developed and applied two complementary methods—one manual based on the marker gene expression, and one automatic based on the similarity between transcriptomic clusters. By applying both methods, we can confidently track the transcriptomes of the same cell type throughout development and study the unique molecular features of each stage. We note that two other methods for tracing transcriptomes of the same neuronal types across development—batch-correction to cluster same cell types across different stages, and training an artificial neural network to classify cell type—have been applied successfully in recent single-cell transcriptome studies of cells in the developing *Drosophila* optic lobe (Kurmangaliyev et al., 2020; Ozel et al., 2020).

Together, those methods can be applied to other single-cell studies where diverse cell types and multiple states are involved. Those methods can be especially useful for tissues with high cellular diversity but lack unique markers for each cell type.

Using single-cell RNAseq data to identify new candidate molecules for future studies

In this study, we have obtained high-quality single-cell transcriptomes of most excitatory PNs from early pupal stage to adulthood (**Figure 1**). We have used combinations of markers and

drivers to decode the transcriptomic identity of 21 transcriptomic clusters at 24h APF (**Figure 2**), and matched clusters representing the same PN type across four developmental stages (**Figure 7**).

Using this rich and well-annotated dataset, researchers can now explore different aspects of PN development and function to identify candidate molecules for future studies. For example, one can search for novel molecules involved in neurite pruning among the differentially expressed genes between the embryonically-born and larval-born PNs at 0h APF (**Figure 4B–D**). Developmentally enriched genes and genes that are differentially expressed among different PN types, on the other hand, can be good candidates for studies on neural development and wiring specificity (**Figure 3** and **Figure 9**). Differentially expressed neuronal signaling genes in adult PNs can be used to explore differences in physiological properties and information processing (**Figure 10**). In addition, driver lines for specific types of PNs can be made using genes that show consistent expression pattern across different stages (**Figure 7—figure supplement 2**) to label and genetically manipulate specific PN types. Together with several recent in depth scRNAseq studies of cells in the visual and olfactory system across multiple stages (Jain et al., 2020; Kurmangaliyev et al., 2020; McLaughlin et al., 2020; Ozel et al., 2020), these studies have established foundations of gene expression for *Drosophila* olfactory and visual systems and should catalyze new biological discoveries.

Methods and Materials

Key Resource Table

Reagent type (species) or resource	Designation	Source or reference	Identifiers	Additional information
Genetic reagent (*D. melanogaster*)	*GH146-GAL4*	(Stocker et al., 1997)	RRID: BDSC_30026	
Genetic reagent (*D. melanogaster*)	*VT033006-GAL4*	(Tirian & Dickson, 2017)	RRID: BDSC_73333	
Genetic reagent (*D. melanogaster*)	*Mz19-GAL4*	(Jefferis et al., 2004)	RRID: BDSC_41573	
Genetic reagent (*D. melanogaster*)	*knot-GAL4*	(Lee et al., 2018)	RRID: BDSC_ 67516	
Genetic reagent (*D. melanogaster*)	*split#28-GAL4*	Yoshi Aso (unpublished)	N/A	SS01265
Genetic reagent (*D. melanogaster*)	*split#7-GAL4*	Yoshi Aso (unpublished)	N/A	SS01867
Genetic reagent (*D. melanogaster*)	*split#15-GAL4*	Yoshi Aso (unpublished)	N/A	SS01165
Genetic reagent (*D. melanogaster*)	*GH146-Flp*	(Hong et al., 2009)	N/A	
Genetic reagent (*D. melanogaster*)	*UAS-FRT-STOP-FRT-mCD8GFP*	(Hong et al., 2009)	RRID: BDSC_30125	
Genetic reagent (*D. melanogaster*)	*zfh2-GAL4*	(Lee et al., 2018)	RRID: BDSC_86479	
Genetic reagent (*D. melanogaster*)	*Act-FRT-STOP-FRT-GAL4*	(Pignoni & Zipursky, 1997)	N/A	
Genetic reagent (*D. melanogaster*)	*UAS-Flp*	(Duffy et al., 1998)	N/A	
Genetic reagent (*D. melanogaster*)	*C15-p65^{AD}*	(Xie et al., 2019)	N/A	
Genetic reagent (*D. melanogaster*)	*C15-GAL4^{DBD}*	This study	N/A	

Genetic reagent (*D. melanogaster*)	*danr-P65^{AD}*	This study	N/A	
Genetic reagent (*D. melanogaster*)	*VT033006-GAL4^{DBD}*	Yoshi Aso (unpublished)	N/A	
Genetic reagent (*D. melanogaster*)	*DIP-zeta-GAL4*	(Cosmanescu et al., 2018)	RRID: BDSC_90317	
Genetic reagent (*D. melanogaster*)	*DIP-eta-GAL4*	(Cosmanescu et al., 2018)	RRID: BDSC_90318	
Genetic reagent (*D. melanogaster*)	*AstA-GAL4*	(Deng et al., 2019)	RRID: BDSC_84593	
Genetic reagent (*D. melanogaster*)	*DIP-beta-GAL4*	(Carrillo et al., 2015)	RRID: BDSC_90316	
Genetic reagent (*D. melanogaster*)	*kn-GAL4^{DBD}*	This study	N/A	
Genetic reagent (*D. melanogaster*)	*elav-GAL4^{DBD}*	(Luan et al., 2006)	N/A	
Antibody	Rat monoclonal anti-Ncad	Developmental Studies Hybridoma Bank	RRID: AB_528121	(1:40 in 5% normal goat serum)
Antibody	Chicken polyclonal anti-GFP	Aves Labs	RRID: AB_10000240	(1:1000 in 5% normal goat serum)
Software, algorithm	ZEN	Carl Zeiss	RRID: SCR_013672	
Software, algorithm	ImageJ	National Institutes of Health	RRID: SCR_003070	
Software, algorithm	Illustrator	Adobe	RRID: SCR_010279	
Software, algorithm	STAR 2.5.4	(Dobin et al., 2013)	RRID: SCR_015899	https://github.com/alexdobin/STAR
Software, algorithm	HTseq 0.11.2	(Anders et al., 2015)	RRID: SCR_005514	https://github.com/htseq/htseq
Software, algorithm	Scanpy	(Wolf et al., 2018)	RRID: SCR_018139	https://scanpy.readthedocs.io/en/stable/
Software, algorithm	Iterative Clustering for Identifying	(Li et al., 2017)	N/A	https://github.com/felixhorns/FlyPN

	Markers (ICIM)			
Recombinant DNA reagent	*pT-GEM(0)* (plasmid)	(Diao et al., 2015)	RRID: Addgene_62891	
Recombinant DNA reagent	*pBS-KS-attB2-SA(2)-T2A-Gal4DBD-Hsp70* (plasmid)	(Diao et al., 2015)	RRID: Addgene_62904	
Recombinant DNA reagent	*pU6-BbsI-chiRNA* (plasmid)	(Gratz et al., 2013)	RRID: Addgene_45946	

Drosophila **Stocks and genotypes**

Flies are maintained on standard cornmeal medium at 25 °C with 12-h light–dark cycle. The following lines were used in this study: *GH146-GAL4* (Stocker et al., 1997), *VT033006-GAL4* (Tirian & Dickson, 2017), *Mz19-GAL4* (Jefferis et al., 2004*)*, *knot-GAL4* (Lee et al., 2018), *GH146-Flp*, *UAS-FRT-STOP-FRT-mCD8-GFP* (Potter et al., 2010), *zfh2-GAL4* (Lee et al., 2018*)*, *Act-FRT-STOP-FRT-GAL4* (Pignoni & Zipursky, 1997), *UAS-Flp* (Duffy et al., 1998), *C15-p65^{AD}* (Xie et al., 2019), *DIP-beta-GAL4*, *DIP-eta-GAL4*, *DIP-zeta-GAL4* (Carrillo et al., 2015; Cosmanescu et al., 2018), *AstA-GAL4* (Deng et al., 2019), and *elav-GAL4^{DBD}* (Luan et al., 2006). *VT033006-GAL4^{DBD}*, split-GAL4 line #7 (SS01867), #15 (SS01165), and #28 (SS01265) are unpublished reagents generously provided by Yoshi Aso (Janelia Research Campus).

Generation of *danr-p65^{AD}*, kn-*GAL4^{DBD}*, and *C15-GAL4^{DBD}*

danr-p65^{AD} was generated using CRISPR mediated knock-in. ~2000 bp of genomic sequence flanking the targeted insertion site was amplified by Q5 hot-start high-fidelity DNA polymerase (New England Biolabs) and inserted into *pCR-Blunt-TOPO* vectors (Thermo Fisher). Using this vector, we generated homology directed repair (HDR) vector *TOPO-danr-T2A-p65AD-P3-RFP* by inserting *T2A-p65(AD)::Zip+* and *3XP3-RFP-SV40* (cloned from *pT-GEM(0)* Addgene #62891) 45bp downstream of the start codon of *danr*. CRISPR guide RNA (gRNA) targeting a sequence inside *danr* (AACATCCGGATGAGCACGCG) were designed by the flyCRISPR Target Finder tool and cloned into a *pU6-BbsI-chiRNA* vector (Addgene #45946). The HDR and gRNA vectors were co-injected into *nos-Cas9* (gift from Dr. Ben White) embryos. RFP+ progenies were selected and individually balanced.

kn-GAL4^{DBD} was generated by co-injecting *pBS-KS-attB2-SA(2)-T2A-GAL4DBD-Hsp70* (Addgene #62904) and ΦC31 into the embryos of *MI15480* (BL61064). All *yellow*$^{-}$ progenies were individually balanced.

C15-GAL4^{DBD} was generated using methods similar to *danr-p65^{AD}*. But because C15 have been shown to be involved in PN dendrite targeting (Li et al., 2017), instead of inserting driver elements into the coding region, the stop codon of *C15* was replaced by *T2A-GAL4(DBD)::Zip+* to prevent disruption of the gene.

Immunofluorescence

Fly brains were dissected and immunostained according to previously described methods (Wu & Luo, 2006). Primary antibodies used in this study included rat anti-Ncad (N-Ex #8; 1:40; Developmental Studies Hybridoma Bank), chicken anti-GFP (1:1000; Aves Labs). Secondary antibodies conjugated to Alexa Fluor 488/647 (Jackson ImmunoResearch) were used at 1:250. 5% normal goat serum in phosphate buffered saline was used for blocking and diluting antibodies. Confocal images were collected with a Zeiss LSM 780 and processed with ImageJ.

Single-cell RNA sequencing procedure

Single-cell RNA sequencing was performed following previously described protocol (Li et al., 2017). Briefly, *Drosophila* brains with mCD8-GFP labeled cells using specific GAL4 drivers were dissected at appropriate timepoints (0–6h APF, 24–30h APF, 48–54h APF, and 1–5 day adults). Optic lobes were removed from brain during dissection for all timepoints except for 0-6h APF. Single-cell suspension were prepared and GFP positive cells were sorted using Fluorescence Activated Cell Sorting (FACS) into individual wells of 384-well plates containing lysis buffer using SH800 (Sony Biotechnology). Full-length poly(A)-tailed RNA was reverse-transcribed and amplified by PCR following the SMART-seq2 protocol (Picelli et al., 2014). cDNA was digested using lambda exonuclease (New England Biolabs) and then amplified for 25 cycles. Sequencing libraries were prepared from amplified cDNA, pooled, and quantified using BioAnalyser (Agilent). Sequencing was performed using the Novaseq 6000 Sequencing system (Illumina) with 100 paired-end reads and 2 x 8 bp index reads.

QUANTIFICATION AND STATISTICAL ANALYSIS

Unless otherwise specified, all data analysis was performed in Python using Scanpy (Wolf et al., 2018), Numpy, Scipy, Pandas, scikit-learn, and custom single-cell RNA-seq modules (Li et al., 2017; Brbic et al., 2020). Gene Ontology analysis were performed using Flymine (Lyne et al., 2007). Sequencing reads and preprocessed sequence data are available in the NCBI Gene Expression Omnibus (GSE161228). Custom analysis code is available at https://github.com/Qijing-Xie/FlyPN_development.

Sequence alignment and preprocessing

Reads were aligned to the *Drosophila melanogaster* genome (r6.10) using STAR (2.5.4) (Dobin et al., 2013). Gene counts were produced using HTseq (0.11.2) with default settings except ‘‘-m intersection-strict’ (Anders et al., 2015). We removed low-quality cells having fewer than 100,000 uniquely mapped reads. To normalize for differences in sequencing depth across individual cells, we rescaled gene counts to counts per million reads (CPM). All analyses were performed after converting gene counts to logarithmic space via the transformation $\text{Log}_2(\text{CPM}+1)$. We further filter out non-neuronal cells by selecting cells with high expression of canonical neuronal genes (*elav*, *brp*, *Syt1*, *nSyb*, *CadN*, and *mCD8-GFP*). We retained cells expressing at least 8 $\text{Log}_2(\text{CPM}+1)$ for least 2/6 markers.

Dimensionality reduction and clustering

To select variable genes for dimensionality reduction, we used previously described methods to search for either overdispersed genes (Satija et al., 2015) or ICIM genes (Li et al., 2017). We then further reduced its dimensionality using tSNE to project the reduced gene expression matrix into a two-dimensional space (van der Maaten & Hinton, 2008). We observed that most of our recently sequenced cells using NovaSeq exhibited some small batch effect with PNs sequenced using NextSeq [PNs from (Li et al., 2017)]. To overcome this batch effect (in Figure 2, and

Figure 7—figure supplement 2 A, C), we performed principal component analysis (PCA) on the ICIM matrix, applied Harmony to correct for batch effect on the principal components (PCs) (Korsunsky et al., 2019), and used tSNE to further project the Harmony-corrected PCs into a two-dimensional space.

To cluster PNs in an unbiased manner, we applied the hierarchical density-based clustering algorithm, HDBSCAN, on the tSNE projection (McInnes et al., 2017). Parameters min_cluster_size and min_samples were adjusted to separate clusters representing different types of PNs. In addition, we also clustered cells using an independent, community-detection method called Leiden on the neighborhood graph computed based on the ICIM gene matrix (Blondel et al., 2008; Levine et al., 2015; McInnes et al., 2018). Both methods appeared to agree with each other for all datasets we examined (examples in Figure 5—figure supplement 1), and we assigned PN types in Figure 2 based on HDBSCAN clustering.

Global level dynamic gene identification

To identify dynamically expressed genes on the global level (Figure 3), we first identified the top 150 most differentially expressed genes (Mann-Whitney U test) between every two stages and combined them to obtain a set of 474 dynamic genes. We calculated the median expression of each gene at each timepoint and normalized these median expression values by dividing them by the maximum value across time points. We then performed dimensionality reduction on the expression profiles of the genes using tSNE, and identified clusters using HDBSCAN on the projected coordinates. This resulted in identification of 8 sets of genes with distinct dynamic profiles, of which 2 sets are upregulated (Figure 3E), 4 sets are down regulated (Figure 3D), and 2 sets without obvious trend from 0h APF to adult cells (data not shown).

Transcriptomic similarity calculation

To analyze the transcriptome differences of PNs in different stages (Figure 4E, F), we first isolated lPNs and adPNs to analyze cells from each lineage separately. Cell-level analysis was performed by calculating for each cell mean inverse Euclidean distance in the 2-dimensional UMAP space from all other cells within each stage using the 1215 genes identified by ICIM from most PNs of all stages (Figure 3A). Box plots show the distance distribution at each stage (Figure 4E and F, left). Cluster-level analysis was performed on the MARS clusters. We identified a set of differentially expressed genes for each cluster and calculated Pearson correlation on differentially expressed genes between all pairs of clusters. Bar plots represent mean values across all pairs and errors are 95% confidence intervals determined by bootstrapping with n=1,000 iterations (Figure 4E and F, right).

PN type identification for most PNs

We observed that the transcriptomes of different PN types are the most distinct at 24h APF and variable genes identified at this stage carry type-specific information (Figure 5). Therefore, we calculated the differentially expressed genes among 24h APF clusters and applied MARS to identify clusters in the space of those genes. MARS is able to reuse annotated single-cell datasets to learn shared low-dimensional space of both annotated and unannotated datasets in which cells are grouped according to their cell types. However, initially we did not have any annotated experiments, so we first applied MARS to annotate 24h APF clusters. We then used 24h APF clusters as annotated dataset and moved to annotate PNs at 48h APF. We then repeated the same procedure by gradually increasing our set of annotated datasets. In particular, we used 24h and

48h APF data to help in annotating 0h APF, and finally all three datasets (0h, 24h, 48h) for the adult PNs. We proceed in this order according to the expected difficulty to identify PN types at a particular stage (Figure 5). At each stage, we ran MARS multiple times with different random initializations and architecture parameters to increase our confidence in the discovered clusters, and combined annotations from these different runs. For each cluster, we additionally manually checked the expressions of known PN markers to confirm the annotations.

Matching clusters representing the same PN type across development using marker expression

For each cluster, we used Mann-Whitney U test to find genes that are highly expressed in that cluster compared to the rest. Then, among those genes, we searched for genes or 2-gene combinations which are uniquely expressed in 1 cluster. We check each gene or combination of genes at the other stages, and if they are also only expressed in 1 cluster and they are of the same lineage, we consider them to be the same types of PNs. Genes used to match clusters representing the same PN types at different timepoints are summarized in a dot-plot in Figure 7—figure supplement 2.

In addition, we used previously sequenced subset of PNs using *Mz19-GAL4* and *kn-GAL4* to overlay with most PNs in combinations of those markers to confirm our matching.

Matching clusters representing the same PN type across development using similarity calculation

For each cluster, we found the set of differentially expressed genes in that cluster compared to all other clusters at the same stage. Next, we computed the similarity of the sets of identified differentially expressed genes between all pairs of clusters across subsequent stages. Specifically, we computed similarity scores between all pairs of clusters from (i) 0h and 24h APF, (ii) 24h and 48h APF, and (iii) 48h and adult APF. The similarity of the sets of differentially expressed genes was computed as the Jaccard similarity index defined as the ratio of the cardinality of the intersection of two sets and the cardinality of the union of the sets. We excluded clusters representing vPNs and APLs for matching most PNs across 4 stages (Figure 7). For each cluster, we then identified its most similar cluster at the adjacent stage according to the Jaccard index. If the clusters between two stages coincide—meaning that two clusters from two stages have the highest similarity to each other, we consider the clusters to be matched. Empirically, we found this matching procedure to be stringent, resulting in high confidence matching pairs.

Correlation between different PN types

MARS clusters of excitatory PNs were used for analysis in Figure 8. We performed PCA on the entire matrix and calculated their correlation based on the PCs. Dendrograms shown in Figure 8—figure supplement 1 are generated using distance calculated using Farthest Point Algorithm and organized so the distance between successive leaves is minimal.

To observe the relationship between birth timing and their transcriptomic similarity, for each stage, we selected adPN clusters, performed PCA among all genes detected, calculated their correlation, and plotted the correlation matrices according to their birth order (Yu et al., 2010) (Figure 8B). For the two clusters representing either VM7 or VM5v PNs, we ordered them based on their correlation with decoded PN types whose birth order are adjacent to either of these two PN types. We are showing adPNs in the figure because we decoded much fewer transcriptomic clusters belonging to the lPN lineage, which is too few to carry out analysis shown in Figure 8

C–D with robust statistical backing. Nevertheless, we still observed higher correlation between lPN types with adjacent birth-order in 0h and 24h APF (data not shown).

Spearman's rank correlation calculation and permutation test

For consistency, 8 adPN types that were decoded across 4 stages were selected for this analysis (Figure 8C). For each PN type X, the group of PNs that are born either earlier or later than X was selected depending on which direction contains more PN types (each group contains at least 5 types of PNs). Then, we ranked the PN types according to their correlation with X and calculated the Spearman's rank correlation of this ranking with the ranking based on their birth order. For each stage, we obtained the average correlation coefficients and plotted the result as a red dot on the x-axis for each timepoint. Higher value indicates higher correlation between birth order and order calculated based on their transcriptomic similarity.

To determine if we can reject the null hypothesis that the adPN transcriptomic similarity do not covary with the ranks of the birth order, we performed permutation test. We randomly shuffled the birth order and performed the aforementioned correlation calculation for 5000 iterations. The distribution of the simulated average correlations is shown in the histogram of Figure 8C. We obtained the p-value by dividing the number of times of the simulated correlation is greater than the observed correlation by the total number of iterations.

Developmental trajectory analysis

Pseudo-time analysis of 0h APF adPNs was performed using the monocle package in R (Trapnell et al., 2014; Qiu et al., 2017; Cao et al., 2019). We selected only adPNs born at larval stage because the embryonically born adPNs have a very distinct transcriptomes which skew clustering. We applied the dimensionality reduction method UMAP (Becht et al., 2018) on 561 24h ICIM genes to resolve distinct PN types. This dimensionally reduced dataset was then used as the basis for a developmental trajectory graph created by Monocle 3. We then selected the cluster representing DL1 PNs to be the root node of the trajectory and computed the pseudo-times based on distance from the root in accordance to the trajectory.

Differential gene expression analysis

We used adPN and lPN clusters to identify differentially expressed genes at each stage (**Figure 9**). We performed Mann-Whitney U test on each cluster compared to the rest of the clusters at each developmental stage and applied Benjamini-Hochberg Procedure to adjust p-value. Genes with an adjusted p-value of less than 0.01 were kept for our analysis.

To identify genes that are transcription factors (TFs), cell surface molecules (CSM), ion channels, and transmembrane receptors, we used curated lists. The TF list was from the FlyTF database (Pfreundt et al., 2010) and the CSM list was from (Kurusu et al., 2008). These lists were manually curated to remove spurious annotations and redundancies according to Flybase annotation. Lists of ion channels and transmembrane receptors were based on gene groups obtained from FlyBase. To avoid redundancy, ion channels that also belong to the transmembrane receptor gene group are not plotted as transmembrane receptors (**Figure 9C**, bottom).

Acknowledgement

We thank Yoshi Aso, Gerald Rubin, Hugo Bellen, Kai Zinn, and Larry Zipursky for the kind gifts of reagents. We thank the Bloomington *Drosophila* Stock Center and the Vienna *Drosophila* Resource Center for fly lines, and Addgene for plasmids. We thank Tom Clandinin, Yanyang Ge, Julia Kaltschmidt, Justus Kebschull, Kang Shen, Andrew Shuster, and all Luo lab members for technical support and insightful advice on this study. We thank Mary Molacavage for administrative assistance.

Additional information

Competing interests

The authors declare that no competing interest exists.

Funding

This work was supported by NIH grant R01 DC005982 (to L.L.) and 1K99AG062746 (to H.L.), and by Wu Tsai Neurosciences Institute at Stanford (Neuro-omics project). Qijing Xie was a Bertarelli Fellow. S.R.Q. is a Chan Zuckerberg Biohub investigator. L.L. is a Howard Hughes Medical Institute investigator. Hongjie Li was a Wu Tsai Neuroscience Institute interdisciplinary postdoctoral scholar.

References

Alyagor, I., Berkun, V., Keren-Shaul, H., Marmor-Kollet, N., David, E., Mayseless, O., Issman-Zecharya, N., Amit, I., & Schuldiner, O. (2018). Combining Developmental and Perturbation-Seq Uncovers Transcriptional Modules Orchestrating Neuronal Remodeling. *Dev Cell, 47*(1), 38-52 e36. doi:10.1016/j.devcel.2018.09.013

Anders, S., Pyl, P. T., & Huber, W. (2015). HTSeq--a Python framework to work with high-throughput sequencing data. *Bioinformatics, 31*(2), 166-169. doi:10.1093/bioinformatics/btu638

Bates, A. S., Schlegel, P., Roberts, R. J. V., Drummond, N., Tamimi, I. F. M., Turnbull, R., Zhao, X., Marin, E. C., Popovici, P. D., Dhawan, S., Jamasb, A., Javier, A., Serratosa Capdevila, L., Li, F., Rubin, G. M., Waddell, S., Bock, D. D., Costa, M., & Jefferis, G. (2020). Complete Connectomic Reconstruction of Olfactory Projection Neurons in the Fly Brain. *Curr Biol, 30*(16), 3183-3199 e3186. doi:10.1016/j.cub.2020.06.042

Becht, E., McInnes, L., Healy, J., Dutertre, C. A., Kwok, I. W. H., Ng, L. G., Ginhoux, F., & Newell, E. W. (2018). Dimensionality reduction for visualizing single-cell data using UMAP. *Nat Biotechnol*. doi:10.1038/nbt.4314

Bhandawat, V., Olsen, S. R., Gouwens, N. W., Schlief, M. L., & Wilson, R. I. (2007). Sensory processing in the Drosophila antennal lobe increases reliability and separability of ensemble odor representations. *Nat Neurosci, 10*(11), 1474-1482. doi:10.1038/nn1976

Blondel, V. D., Guillaume, J. L., Lambiotte, R., & Lefebvre, E. (2008). Fast unfolding of communities in large networks. *Journal of Statistical Mechanics-Theory and Experiment*. doi:Artn P10008

10.1088/1742-5468/2008/10/P10008

Brbic, M., Zitnik, M., Wang, S., Pisco, A. O., Altman, R. B., Darmanis, S., & Leskovec, J. (2020). MARS: discovering novel cell types across heterogeneous single-cell experiments. *Nat Methods*. doi:10.1038/s41592-020-00979-3

Cao, J., Spielmann, M., Qiu, X., Huang, X., Ibrahim, D. M., Hill, A. J., Zhang, F., Mundlos, S., Christiansen, L., Steemers, F. J., Trapnell, C., & Shendure, J. (2019). The single-cell

748 transcriptional landscape of mammalian organogenesis. *Nature, 566*(7745), 496-502.
749 doi:10.1038/s41586-019-0969-x
750 Carrillo, R. A., Ozkan, E., Menon, K. P., Nagarkar-Jaiswal, S., Lee, P. T., Jeon, M., Birnbaum,
751 M. E., Bellen, H. J., Garcia, K. C., & Zinn, K. (2015). Control of Synaptic Connectivity
752 by a Network of Drosophila IgSF Cell Surface Proteins. *Cell, 163*(7), 1770-1782.
753 doi:10.1016/j.cell.2015.11.022
754 Cembrowski, M. S., & Menon, V. (2018). Continuous Variation within Cell Types of the
755 Nervous System. *Trends Neurosci, 41*(6), 337-348. doi:10.1016/j.tins.2018.02.010
756 Cosmanescu, F., Katsamba, P. S., Sergeeva, A. P., Ahlsen, G., Patel, S. D., Brewer, J. J., Tan, L.,
757 Xu, S., Xiao, Q., Nagarkar-Jaiswal, S., Nern, A., Bellen, H. J., Zipursky, S. L., Honig, B.,
758 & Shapiro, L. (2018). Neuron-Subtype-Specific Expression, Interaction Affinities, and
759 Specificity Determinants of DIP/Dpr Cell Recognition Proteins. *Neuron, 100*(6), 1385-
760 1400 e1386. doi:10.1016/j.neuron.2018.10.046
761 Deng, B., Li, Q., Liu, X., Cao, Y., Li, B., Qian, Y., Xu, R., Mao, R., Zhou, E., Zhang, W., Huang,
762 J., & Rao, Y. (2019). Chemoconnectomics: Mapping Chemical Transmission in
763 Drosophila. *Neuron, 101*(5), 876-893 e874. doi:10.1016/j.neuron.2019.01.045
764 Diao, F., Ironfield, H., Luan, H., Diao, F., Shropshire, W. C., Ewer, J., Marr, E., Potter, C. J.,
765 Landgraf, M., & White, B. H. (2015). Plug-and-play genetic access to drosophila cell
766 types using exchangeable exon cassettes. *Cell Rep, 10*(8), 1410-1421.
767 doi:10.1016/j.celrep.2015.01.059
768 Dionne, H., Hibbard, K. L., Cavallaro, A., Kao, J. C., & Rubin, G. M. (2018). Genetic Reagents
769 for Making Split-GAL4 Lines in Drosophila. *Genetics, 209*(1), 31-35.
770 doi:10.1534/genetics.118.300682
771 Dobin, A., Davis, C. A., Schlesinger, F., Drenkow, J., Zaleski, C., Jha, S., Batut, P., Chaisson,
772 M., & Gingeras, T. R. (2013). STAR: ultrafast universal RNA-seq aligner. *Bioinformatics,*
773 *29*(1), 15-21. doi:10.1093/bioinformatics/bts635
774 Duffy, J. B., Harrison, D. A., & Perrimon, N. (1998). Identifying loci required for follicular
775 patterning using directed mosaics. *Development, 125*(12), 2263-2271. Retrieved from
776 https://www.ncbi.nlm.nih.gov/pubmed/9584125
777 Elkahlah, N. A., Rogow, J. A., Ahmed, M., & Clowney, E. J. (2020). Presynaptic developmental
778 plasticity allows robust sparse wiring of the Drosophila mushroom body. *Elife, 9*.
779 doi:10.7554/eLife.52278
780 Gratz, S. J., Wildonger, J., Harrison, M. M., & O'Connor-Giles, K. M. (2013). CRISPR/Cas9-
781 mediated genome engineering and the promise of designer flies on demand. *Fly (Austin),*
782 *7*(4), 249-255. doi:10.4161/fly.26566
783 Hie, B., Bryson, B., & Berger, B. (2019). Efficient integration of heterogeneous single-cell
784 transcriptomes using Scanorama. *Nat Biotechnol, 37*(6), 685-691. doi:10.1038/s41587-
785 019-0113-3
786 Holguera, I., & Desplan, C. (2018). Neuronal specification in space and time. *Science, 362*(6411),
787 176-180. doi:10.1126/science.aas9435
788 Hong, W., & Luo, L. (2014). Genetic control of wiring specificity in the fly olfactory system.
789 *Genetics, 196*(1), 17-29. doi:10.1534/genetics.113.154336
790 Hong, W., Mosca, T. J., & Luo, L. (2012). Teneurins instruct synaptic partner matching in an
791 olfactory map. *Nature, 484*(7393), 201-207. doi:10.1038/nature10926

Hong, W., Zhu, H., Potter, C. J., Barsh, G., Kurusu, M., Zinn, K., & Luo, L. (2009). Leucine-rich repeat transmembrane proteins instruct discrete dendrite targeting in an olfactory map. *Nat Neurosci, 12*(12), 1542-1550. doi:10.1038/nn.2442

Inada, K., Tsuchimoto, Y., & Kazama, H. (2017). Origins of Cell-Type-Specific Olfactory Processing in the Drosophila Mushroom Body Circuit. *Neuron, 95*(2), 357-367 e354. doi:10.1016/j.neuron.2017.06.039

Jain, S., Lin, Y., Kurmangaliyev, Y., Mirshahidi, P., Parrington, B., & Zipursky, S. L. (2020). A Global Temporal Genetic Program for Neural Circuit Formation. *BioRxiv*.

Jan, Y. N., & Jan, L. Y. (1994). Genetic control of cell fate specification in Drosophila peripheral nervous system. *Annu Rev Genet, 28*, 373-393. doi:10.1146/annurev.ge.28.120194.002105

Jan, Y. N., & Jan, L. Y. (2010). Branching out: mechanisms of dendritic arborization. *Nat Rev Neurosci, 11*(5), 316-328. doi:10.1038/nrn2836

Jeanne, J. M., Fisek, M., & Wilson, R. I. (2018). The Organization of Projections from Olfactory Glomeruli onto Higher-Order Neurons. *Neuron, 98*(6), 1198-1213 e1196. doi:10.1016/j.neuron.2018.05.011

Jefferis, G. S., Marin, E. C., Stocker, R. F., & Luo, L. (2001). Target neuron prespecification in the olfactory map of Drosophila. *Nature, 414*(6860), 204-208. doi:10.1038/35102574

Jefferis, G. S., Potter, C. J., Chan, A. M., Marin, E. C., Rohlfing, T., Maurer, C. R., Jr., & Luo, L. (2007). Comprehensive maps of Drosophila higher olfactory centers: spatially segregated fruit and pheromone representation. *Cell, 128*(6), 1187-1203. doi:10.1016/j.cell.2007.01.040

Jefferis, G. S., Vyas, R. M., Berdnik, D., Ramaekers, A., Stocker, R. F., Tanaka, N. K., Ito, K., & Luo, L. (2004). Developmental origin of wiring specificity in the olfactory system of Drosophila. *Development, 131*(1), 117-130. doi:10.1242/dev.00896

Jenett, A., Rubin, G. M., Ngo, T. T., Shepherd, D., Murphy, C., Dionne, H., Pfeiffer, B. D., Cavallaro, A., Hall, D., Jeter, J., Iyer, N., Fetter, D., Hausenfluck, J. H., Peng, H., Trautman, E. T., Svirskas, R. R., Myers, E. W., Iwinski, Z. R., Aso, Y., DePasquale, G. M., Enos, A., Hulamm, P., Lam, S. C., Li, H. H., Laverty, T. R., Long, F., Qu, L., Murphy, S. D., Rokicki, K., Safford, T., Shaw, K., Simpson, J. H., Sowell, A., Tae, S., Yu, Y., & Zugates, C. T. (2012). A GAL4-driver line resource for Drosophila neurobiology. *Cell Rep, 2*(4), 991-1001. doi:10.1016/j.celrep.2012.09.011

Johnston, R. J., Jr., & Desplan, C. (2010). Stochastic mechanisms of cell fate specification that yield random or robust outcomes. *Annu Rev Cell Dev Biol, 26*, 689-719. doi:10.1146/annurev-cellbio-100109-104113

Kalish, B. T., Cheadle, L., Hrvatin, S., Nagy, M. A., Rivera, S., Crow, M., Gillis, J., Kirchner, R., & Greenberg, M. E. (2018). Single-cell transcriptomics of the developing lateral geniculate nucleus reveals insights into circuit assembly and refinement. *Proc Natl Acad Sci U S A, 115*(5), E1051-E1060. doi:10.1073/pnas.1717871115

Kirilly, D., Gu, Y., Huang, Y., Wu, Z., Bashirullah, A., Low, B. C., Kolodkin, A. L., Wang, H., & Yu, F. (2009). A genetic pathway composed of Sox14 and Mical governs severing of dendrites during pruning. *Nat Neurosci, 12*(12), 1497-1505. doi:10.1038/nn.2415

Kirilly, D., Wong, J. J., Lim, E. K., Wang, Y., Zhang, H., Wang, C., Liao, Q., Wang, H., Liou, Y. C., Wang, H., & Yu, F. (2011). Intrinsic epigenetic factors cooperate with the steroid hormone ecdysone to govern dendrite pruning in Drosophila. *Neuron, 72*(1), 86-100. doi:10.1016/j.neuron.2011.08.003

Kohwi, M., & Doe, C. Q. (2013). Temporal fate specification and neural progenitor competence during development. *Nat Rev Neurosci, 14*(12), 823-838. doi:10.1038/nrn3618

Kolodkin, A. L., & Tessier-Lavigne, M. (2011). Mechanisms and molecules of neuronal wiring: a primer. *Cold Spring Harb Perspect Biol, 3*(6). doi:10.1101/cshperspect.a001727

Korsunsky, I., Millard, N., Fan, J., Slowikowski, K., Zhang, F., Wei, K., Baglaenko, Y., Brenner, M., Loh, P. R., & Raychaudhuri, S. (2019). Fast, sensitive and accurate integration of single-cell data with Harmony. *Nat Methods, 16*(12), 1289-1296. doi:10.1038/s41592-019-0619-0

Kurmangaliyev, Y. Z., Yoo, J., Valdes-Aleman, J., Sanfilippo, P., & Zipursky, S. L. (2020). Transcriptional Programs of Circuit Assembly in the Drosophila Visual System. *Neuron*. doi:10.1016/j.neuron.2020.10.006

Kurusu, M., Cording, A., Taniguchi, M., Menon, K., Suzuki, E., & Zinn, K. (2008). A screen of cell-surface molecules identifies leucine-rich repeat proteins as key mediators of synaptic target selection. *Neuron, 59*(6), 972-985. doi:10.1016/j.neuron.2008.07.037

Lai, S. L., Awasaki, T., Ito, K., & Lee, T. (2008). Clonal analysis of Drosophila antennal lobe neurons: diverse neuronal architectures in the lateral neuroblast lineage. *Development, 135*(17), 2883-2893. doi:10.1242/dev.024380

Lee, P. T., Zirin, J., Kanca, O., Lin, W. W., Schulze, K. L., Li-Kroeger, D., Tao, R., Devereaux, C., Hu, Y., Chung, V., Fang, Y., He, Y., Pan, H., Ge, M., Zuo, Z., Housden, B. E., Mohr, S. E., Yamamoto, S., Levis, R. W., Spradling, A. C., Perrimon, N., & Bellen, H. J. (2018). A gene-specific T2A-GAL4 library for Drosophila. *Elife, 7*. doi:10.7554/eLife.35574

Lee, T., & Luo, L. (1999). Mosaic analysis with a repressible cell marker for studies of gene function in neuronal morphogenesis. *Neuron, 22*(3), 451-461. doi:10.1016/s0896-6273(00)80701-1

Lee, T., Marticke, S., Sung, C., Robinow, S., & Luo, L. (2000). Cell-autonomous requirement of the USP/EcR-B ecdysone receptor for mushroom body neuronal remodeling in Drosophila. *Neuron, 28*(3), 807-818. doi:10.1016/s0896-6273(00)00155-0

Levine, J. H., Simonds, E. F., Bendall, S. C., Davis, K. L., Amir el, A. D., Tadmor, M. D., Litvin, O., Fienberg, H. G., Jager, A., Zunder, E. R., Finck, R., Gedman, A. L., Radtke, I., Downing, J. R., Pe'er, D., & Nolan, G. P. (2015). Data-Driven Phenotypic Dissection of AML Reveals Progenitor-like Cells that Correlate with Prognosis. *Cell, 162*(1), 184-197. doi:10.1016/j.cell.2015.05.047

Levine, R. B., Morton, D. B., & Restifo, L. L. (1995). Remodeling of the insect nervous system. *Curr Opin Neurobiol, 5*(1), 28-35. doi:10.1016/0959-4388(95)80083-2

Li, H. (2020). Single-cell RNA sequencing in Drosophila: Technologies and applications. *Wiley Interdiscip Rev Dev Biol*, e396. doi:10.1002/wdev.396

Li, H., Horns, F., Wu, B., Xie, Q., Li, J., Li, T., Luginbuhl, D. J., Quake, S. R., & Luo, L. (2017). Classifying Drosophila Olfactory Projection Neuron Subtypes by Single-Cell RNA Sequencing. *Cell, 171*(5), 1206-1220 e1222. doi:10.1016/j.cell.2017.10.019

Li, H., Li, T., Horns, F., Li, J., Xie, Q., Xu, C., Wu, B., Kebschull, J. M., McLaughlin, C. N., Kolluru, S. S., Jones, R. C., Vacek, D., Xie, A., Luginbuhl, D. J., Quake, S. R., & Luo, L. (2020a). Single-Cell Transcriptomes Reveal Diverse Regulatory Strategies for Olfactory Receptor Expression and Axon Targeting. *Curr Biol, 30*(7), 1189-1198 e1185. doi:10.1016/j.cub.2020.01.049

Li, H., Shuster, S. A., Li, J., & Luo, L. (2018). Linking neuronal lineage and wiring specificity. *Neural Dev, 13*(1), 5. doi:10.1186/s13064-018-0102-0

Li, J., Han, S., Li, H., Udeshi, N. D., Svinkina, T., Mani, D. R., Xu, C., Guajardo, R., Xie, Q., Li, T., Luginbuhl, D. J., Wu, B., McLaughlin, C. N., Xie, A., Kaewsapsak, P., Quake, S. R., Carr, S. A., Ting, A. Y., & Luo, L. (2020b). Cell-Surface Proteomic Profiling in the Fly Brain Uncovers Wiring Regulators. *Cell, 180*(2), 373-386 e315. doi:10.1016/j.cell.2019.12.029

Liang, L., Li, Y. L., Potter, C. J., Yizhar, O., Deisseroth, K., Tsien, R. W., & Luo, L. Q. (2013). GABAergic Projection Neurons Route Selective Olfactory Inputs to Specific Higher-Order Neurons. *Neuron, 79*(5), 917-931. doi:10.1016/j.neuron.2013.06.014

Lin, S., Kao, C. F., Yu, H. H., Huang, Y., & Lee, T. (2012). Lineage analysis of Drosophila lateral antennal lobe neurons reveals notch-dependent binary temporal fate decisions. *PLoS Biol, 10*(11), e1001425. doi:10.1371/journal.pbio.1001425

Liu, Z., Yang, C. P., Sugino, K., Fu, C. C., Liu, L. Y., Yao, X., Lee, L. P., & Lee, T. (2015). Opposing intrinsic temporal gradients guide neural stem cell production of varied neuronal fates. *Science, 350*(6258), 317-320. doi:10.1126/science.aad1886

Luan, H., Peabody, N. C., Vinson, C. R., & White, B. H. (2006). Refined spatial manipulation of neuronal function by combinatorial restriction of transgene expression. *Neuron, 52*(3), 425-436. doi:10.1016/j.neuron.2006.08.028

Luo, L. (2020). *Principles of Neurobiology* (Second Edition). Boca Raton: Garland Science.

Lyne, R., Smith, R., Rutherford, K., Wakeling, M., Varley, A., Guillier, F., Janssens, H., Ji, W., McLaren, P., North, P., Rana, D., Riley, T., Sullivan, J., Watkins, X., Woodbridge, M., Lilley, K., Russell, S., Ashburner, M., Mizuguchi, K., & Micklem, G. (2007). FlyMine: an integrated database for Drosophila and Anopheles genomics. *Genome Biol, 8*(7), R129. doi:10.1186/gb-2007-8-7-r129

Marin, E. C., Jefferis, G. S., Komiyama, T., Zhu, H., & Luo, L. (2002). Representation of the glomerular olfactory map in the Drosophila brain. *Cell, 109*(2), 243-255. doi:10.1016/s0092-8674(02)00700-6

Marin, E. C., Watts, R. J., Tanaka, N. K., Ito, K., & Luo, L. (2005). Developmentally programmed remodeling of the Drosophila olfactory circuit. *Development, 132*(4), 725-737. doi:10.1242/dev.01614

McInnes, L., Healy, J., & Astels, S. (2017). hdbscan: Hierarchical density based clustering. *Journal of Open Source Software, 2*(11), 205.

McInnes, L., Healy, J., & Melville, J. (2018). Umap: Uniform manifold approximation and projection for dimension reduction. *arXiv preprint arXiv:1802.03426*.

McLaughlin, C. N., Brbic, M., Xie, Q., Li, T., Horns, F., Kolluru, S. S., Kebschull, J. M., Vacek, D., Xie, A., & Li, J. (2020). Single-cell transcriptomes of developing and adult olfactory receptor neurons in Drosophila. *BioRxiv*.

Ozel, M. N., Simon, F., Jafari, S., Holguera, I., Chen, Y. C., Benhra, N., El-Danaf, R. N., Kapuralin, K., Malin, J. A., Konstantinides, N., & Desplan, C. (2020). Neuronal diversity and convergence in a visual system developmental atlas. *Nature*. doi:10.1038/s41586-020-2879-3

Parnas, M., Lin, A. C., Huetteroth, W., & Miesenbock, G. (2013). Odor discrimination in Drosophila: from neural population codes to behavior. *Neuron, 79*(5), 932-944. doi:10.1016/j.neuron.2013.08.006

Pfreundt, U., James, D. P., Tweedie, S., Wilson, D., Teichmann, S. A., & Adryan, B. (2010). FlyTF: improved annotation and enhanced functionality of the Drosophila transcription

929 factor database. *Nucleic Acids Res*, *38*(Database issue), D443-447.
930 doi:10.1093/nar/gkp910
931 Picelli, S., Faridani, O. R., Bjorklund, A. K., Winberg, G., Sagasser, S., & Sandberg, R. (2014).
932 Full-length RNA-seq from single cells using Smart-seq2. *Nat Protoc*, *9*(1), 171-181.
933 doi:10.1038/nprot.2014.006
934 Pignoni, F., & Zipursky, S. L. (1997). Induction of Drosophila eye development by
935 decapentaplegic. *Development*, *124*(2), 271-278. Retrieved from
936 https://www.ncbi.nlm.nih.gov/pubmed/9053304
937 Polanski, K., Young, M. D., Miao, Z., Meyer, K. B., Teichmann, S. A., & Park, J. E. (2020).
938 BBKNN: fast batch alignment of single cell transcriptomes. *Bioinformatics*, *36*(3), 964-
939 965. doi:10.1093/bioinformatics/btz625
940 Potter, C. J., Tasic, B., Russler, E. V., Liang, L., & Luo, L. (2010). The Q system: a repressible
941 binary system for transgene expression, lineage tracing, and mosaic analysis. *Cell*, *141*(3),
942 536-548. doi:10.1016/j.cell.2010.02.025
943 Qiu, X., Mao, Q., Tang, Y., Wang, L., Chawla, R., Pliner, H. A., & Trapnell, C. (2017).
944 Reversed graph embedding resolves complex single-cell trajectories. *Nat Methods*,
945 *14*(10), 979-982. doi:10.1038/nmeth.4402
946 Sanes, J. R., & Yamagata, M. (2009). Many paths to synaptic specificity. *Annu Rev Cell Dev*
947 *Biol*, *25*, 161-195. doi:10.1146/annurev.cellbio.24.110707.175402
948 Sanes, J. R., & Zipursky, S. L. (2020). Synaptic Specificity, Recognition Molecules, and
949 Assembly of Neural Circuits. *Cell*, *181*(6), 1434-1435. doi:10.1016/j.cell.2020.05.046
950 Satija, R., Farrell, J. A., Gennert, D., Schier, A. F., & Regev, A. (2015). Spatial reconstruction of
951 single-cell gene expression data. *Nat Biotechnol*, *33*(5), 495-502. doi:10.1038/nbt.3192
952 Schubiger, M., Wade, A. A., Carney, G. E., Truman, J. W., & Bender, M. (1998). Drosophila
953 EcR-B ecdysone receptor isoforms are required for larval molting and for neuron
954 remodeling during metamorphosis. *Development*, *125*(11), 2053-2062. Retrieved from
955 https://www.ncbi.nlm.nih.gov/pubmed/9570770
956 Stocker, R. F., Heimbeck, G., Gendre, N., & de Belle, J. S. (1997). Neuroblast ablation in
957 Drosophila P[GAL4] lines reveals origins of olfactory interneurons. *J Neurobiol*, *32*(5),
958 443-456. doi:10.1002/(sici)1097-4695(199705)32:5<443::aid-neu1>3.0.co;2-5
959 Tanaka, N. K., Suzuki, E., Dye, L., Ejima, A., & Stopfer, M. (2012). Dye fills reveal additional
960 olfactory tracts in the protocerebrum of wild-type Drosophila. *J Comp Neurol*, *520*(18),
961 4131-4140. doi:10.1002/cne.23149
962 Tasic, B. (2018). Single cell transcriptomics in neuroscience: cell classification and beyond. *Curr*
963 *Opin Neurobiol*, *50*, 242-249. doi:10.1016/j.conb.2018.04.021
964 Thummel, C. S. (1996). Flies on steroids--Drosophila metamorphosis and the mechanisms of
965 steroid hormone action. *Trends Genet*, *12*(8), 306-310. doi:10.1016/0168-
966 9525(96)10032-9
967 Tirian, L., & Dickson, B. J. (2017). The VT GAL4, LexA, and split-GAL4 driver line collections
968 for targeted expression in the Drosophila nervous system. *BioRxiv*, 198648.
969 Traag, V. A., Waltman, L., & van Eck, N. J. (2019). From Louvain to Leiden: guaranteeing well-
970 connected communities. *Sci Rep*, *9*(1), 5233. doi:10.1038/s41598-019-41695-z
971 Trapnell, C., Cacchiarelli, D., Grimsby, J., Pokharel, P., Li, S., Morse, M., Lennon, N. J., Livak,
972 K. J., Mikkelsen, T. S., & Rinn, J. L. (2014). The dynamics and regulators of cell fate
973 decisions are revealed by pseudotemporal ordering of single cells. *Nat Biotechnol*, *32*(4),
974 381-386. doi:10.1038/nbt.2859

van der Maaten, L., & Hinton, G. (2008). Visualizing Data using t-SNE. *Journal of Machine Learning Research, 9*, 2579-2605. Retrieved from <Go to ISI>://WOS:000262637600007

Vosshall, L. B., & Stocker, R. F. (2007). Molecular architecture of smell and taste in Drosophila. *Annu Rev Neurosci, 30*, 505-533. doi:10.1146/annurev.neuro.30.051606.094306

Wilson, R. I. (2013). Early olfactory processing in Drosophila: mechanisms and principles. *Annu Rev Neurosci, 36*, 217-241. doi:10.1146/annurev-neuro-062111-150533

Wolf, F. A., Angerer, P., & Theis, F. J. (2018). SCANPY: large-scale single-cell gene expression data analysis. *Genome Biol, 19*(1), 15. doi:10.1186/s13059-017-1382-0

Wong, J. J., Li, S., Lim, E. K., Wang, Y., Wang, C., Zhang, H., Kirilly, D., Wu, C., Liou, Y. C., Wang, H., & Yu, F. (2013). A Cullin1-based SCF E3 ubiquitin ligase targets the InR/PI3K/TOR pathway to regulate neuronal pruning. *PLoS Biol, 11*(9), e1001657. doi:10.1371/journal.pbio.1001657

Wu, J. S., & Luo, L. (2006). A protocol for dissecting Drosophila melanogaster brains for live imaging or immunostaining. *Nat Protoc, 1*(4), 2110-2115. doi:10.1038/nprot.2006.336

Xie, Q., Wu, B., Li, J., Xu, C., Li, H., Luginbuhl, D. J., Wang, X., Ward, A., & Luo, L. (2019). Transsynaptic Fish-lips signaling prevents misconnections between nonsynaptic partner olfactory neurons. *Proc Natl Acad Sci U S A, 116*(32), 16068-16073. doi:10.1073/pnas.1905832116

Yu, H. H., Kao, C. F., He, Y., Ding, P., Kao, J. C., & Lee, T. (2010). A complete developmental sequence of a Drosophila neuronal lineage as revealed by twin-spot MARCM. *PLoS Biol, 8*(8). doi:10.1371/journal.pbio.1000461

Zeng, H., & Sanes, J. R. (2017). Neuronal cell-type classification: challenges, opportunities and the path forward. *Nat Rev Neurosci, 18*(9), 530-546. doi:10.1038/nrn.2017.85

Zhong, S., Zhang, S., Fan, X., Wu, Q., Yan, L., Dong, J., Zhang, H., Li, L., Sun, L., Pan, N., Xu, X., Tang, F., Zhang, J., Qiao, J., & Wang, X. (2018). A single-cell RNA-seq survey of the developmental landscape of the human prefrontal cortex. *Nature, 555*(7697), 524-528. doi:10.1038/nature25980

Figure legends

Figure 1. Overview of single-cell transcriptomic profiling of *Drosophila* olfactory projection neurons (PNs).

(A) Schematic of the adult *Drosophila* olfactory system. Approximately 50 types of olfactory receptor neurons (ORNs) form one-to-one synaptic connections with 50 types of excitatory PNs at 50 glomeruli in the antennal lobe. Illustrated are two types each of ORNs (brown) and PNs (green), as well as two glomeruli to which their axons and dendrites target. **(B)** Schematic of the developmental process of the adult *Drosophila* olfactory system. The ~50 types of uniglomerular excitatory PNs are from either anterodorsal (adPN) or lateral (lPN) neuroblast lineages. PNs with cell body on the ventral side are inhibitory ventral PNs (vPNs). **(C)** Representative confocal images of PNs from four different developmental stages, 0h APF, 24h APF, 48h APF, and adult. APF: after puparium formation. Images are shown as maximum z-projections of confocal stacks. Antenna lobe is outlined. Scale bars, 40 μm. **(D)** Workflow of the single-cell RNA sequencing using plate-based SMART-seq2. FACS: fluorescence-activated cell sorting. **(E)** Summary of the number of high-quality PNs sequenced at each timepoint and driver lines used. Most PNs refer to PNs sequenced using either *GH146-GAL4* or *VT033006-GAL4*. **(F)** Visualization of all sequenced PNs from four different developmental stages using tSNE plot. Dimensionality reduction was performed using the top 500 overdispersed genes identified from all sequenced PNs.

Figure 1—figure supplement 1. Technical characteristics of PN scRNA-seq.

(A) Representative confocal image and illustration of cells labeled by *GH146-GAL4* at 0h APF. Other than PNs and a pair of APL neurons in the central brain (arrowheads), many cells in the optic lobes (*) are also labeled. **(B)** Representative confocal image and illustration of cells labeled by *VT033006-GAL4* at 0h APF. This driver labels excitatory PNs, but not cells in the optic lobes or vPN or APL neurons. Scale bars, 40 μm. **(C)** Distribution of the number of uniquely mapped reads per cell. **(D)** Distribution of the number of detected genes per cell. **(E)** Heatmaps showing the expression of: *mCD8-GFP*, pan-neuronal makers (*nSyb*, *elav*, *CadN*, *Syt1*, and *brp*), PN marker (*Oaz*), and glial markers (*repo* and *alrm*). Expression levels are indicated by the color bar (CPM, transcript counts per million).

Figure 2. Matching 15 transcriptomic clusters to specific PN types at 24h APF.

(A) Representative maximum z-projection of confocal stacks of *split#28-GAL4* in adults. Dendrites of *split#28-GAL4+* PNs target the DC3 and DA4l glomeruli. **(B)** Diagram of *split#28-GAL4+* PNs. **(C)** tSNE plot showing newly sequenced *split#28-GAL4+* PNs, which form two clusters that can be assigned to DC3 and DA4l PNs (see also Figure 2—figure supplement 1). **(D)** Representative confocal images of *split#7-GAL4* labeled PNs using permanent labeling strategy. One anterior section and one posterior section of the antennal lobe are shown. Using permanent labeling, we found that this driver is expressed in 8 PN types. Genotype: *split#7-GAL4, UAS-Flp, Actin promoter-FRT-STOP-FRT-GAL4, UAS-mCD8-GFP*. **(E)** Diagram of *split#7-GAL4+* PNs. *split#7-GAL4* labels 8 types of PNs. 4 from the adPN lineage (green letters) and 4 from the lPN lineage (red letters). **(F)** tSNE plot of *split#7-GAL4* PNs with *GH146+* PNs (see Figure 2—figure supplement 2 for details on the decoding procedure). **(G)** Representative maximum z-projection of confocal stacks of *kn+* PNs in the adult. *kn-GAL4* was intersected with *GH146-Flp* to restrict the expression of GAL4 in only PNs. **(H)** Representative confocal images of *split#15-*

GAL4 in adults, which labels 2 *kn+* PN types. **(I)** Diagram showing that *kn+* PNs include 6 types of adPNs and two vPNs. **(J)** tSNE plot of *kn-GAL4* PNs with *GH146+* PNs (see Figure 2—figure supplement 3 for details on the decoding procedure). **(K)** Dot plot summarizing drivers and marker genes we used to map 21 transcriptomic clusters to 20 PN types [14 adPNs, 5 lPNs—DA1 PNs form two clusters, one *fru+* and one *fru–* (Li et al., 2017)—and 1 vPNs] and the anterior paired lateral (APL) neurons at 24h APF. Gene expression level [$\log_2$(CPM+1)] is shown by the dot color, and percentages of cells expressing a marker are shown by dot size. **(L)** tSNE plot showing 24h APF PNs colored by PN types (*GH146+* PNs with *split#7+/ split#28* PNs to increase cell number in some less abundant PN types*)*. Scale bars, 20 μm. Axes, D (dorsal), L (lateral). In panel B, E, and I, orange glomeruli represent PN types of unknown transcriptomic identity prior to this study. Green glomeruli represent PN types whose transcriptomic identity were previously decoded. Note that the positions of cells on a tSNE plot are dependent on the random initialization of the program as well as every cell present in the dataset, therefore the position of *GH146+* PNs clusters are different when we plot them with different set of newly sequenced PNs (gray in panels C, F, and J).

Figure 2—figure supplement 1. Validation of DA4l PN identity.
(A) Visualization of *GH146+* and *split#28-GAL4+* PNs using tSNE. Cells are colored according to driver genotypes (left) or by the expression of *zfh2* (right). **(B)** *zfh2-GAL4*, after intersecting with *GH146-Flp*, labels DA4l PNs. Scale bars, 20 μm. Axes, D (dorsal), L (lateral).

Figure 2—figure supplement 2. Decoding *split#7+* PNs.
(A) Representative confocal images of *split#7+* PNs. Without permanent labeling, this driver is strongly expressed in 3 PN types in adults. Permanent labeling showed that it can label 8 adult PN types (Figure 2D), suggesting that this driver is expressed in 8 PN types during development and turned off in 5 of them in adult stage. **(B)** Visualization of *GH146+* and *split#7+* PNs colored according to genotype (left), *acj6* (middle), and *CG31676* (right) expression. Previously, we know among those *split#7+* PNs, the cells with *CG31676* expression are DA1 PNs (Li et al. 2017). **(C)** Among *split#7+* adPN clusters (circled in green), only one cluster does not express *C15*. Intersection between *C15-p65^{AD}* and the GAL4 DNA-binding domain (DBD) from *split#7* (top) as well as intersection between *C15-GAL4^{DBD}* and the p65-activating domain (AD) from *split#7* (bottom) revealed that the *C15* negative cluster represents DL1 PNs. **(D)** Among *split#7+* adPNs (circled in green), two clusters are *danr–*. One of those cluster represents DL1 PNs. Intersection between *danr-p65^{AD}* and *VT033006-GAL4^{DBD}* (split-GAL4 with PN specific expression) revealed the other *danr–* adPN is VA6 PNs. **(E)** One *split#7+* cluster specifically expresses *DIP-zeta*. Intersection between *DIP-zeta-GAL4* and *GH146-Flp* revealed this cluster represents VA2 PNs. As three out of four adPN clusters are assigned, we assigned the last unassigned to be DA3 PNs. **(F)** Among *split#7+* lPNs (circled in red), only one cluster is *DIP-eta-*. Intersection between *DIP-eta-GAL4* and *GH146-Flp* revealed the identity of this cluster as VA5 PNs. **(G)** The *DIP-eta–* cluster also specifically expresses *AstA*. Intersection between *AstA-GAL4* and *GH146-Flp* labels VA5 PNs, further confirming its identity. **(H)** Among the last two unmapped clusters, one is *DIP-beta+*. Intersection between *DIP-beta-GAL4* and *GH146-Flp* revealed the cluster negative for *DIP-beta* is DM2 PNs. And we assigned the remaining *split#7+* lPN cluster to be VC2 PNs. Scale bars, 20 μm. Axes, D (dorsal), L (lateral).

Figure 2—figure supplement 3. Decoding the identity of *kn+* PNs.

(A) *kn* is expressed in 7 transcriptomic cluster in *GH146+* PNs at 24h APF. **(B)** Visualization of *kn+* and *split#15-GAL4+* PNs at 24h APF using tSNE. *kn+* PNs (green) form 8 clusters, two of them intermingled with *split#15-GAL4+* PNs (purple). These 8 clusters are assigned to specific PN types using information in the following panels. **(C)** Summary of marker genes used to decode the identity of *kn-GAL4+* PNs. *trol+* cluster represents VM2 PNs (Li et al., 2007). **(D)** Intersection between *kn-GAL4*^{DBD} and *danr-p65*^{AD} with *GH146-Flp* revealed that the cluster positive for both *kn* and *danr* is VA1v PNs. **(E)** Intersection between *C15-p65*^{AD} and *elav-GAL4*^{DBD} revealed that the cluster positive for *acj6* but negative for *C15* is D PNs. **(F)** Visualization of *DIP-beta* expression among *GH146+* PNs. DA1 lPNs does not express *DIP-beta*. **(G)** Visualization of *DIP-beta* expression among *kn+* PNs. One vPN cluster expresses *DIP-beta*. **(H)** Representative confocal image of *DIP-beta-GAL4* after intersecting with *GH146-Flp*. Innervation of the DA1 glomerulus indicated the *DIP-beta+* vPN cluster is vPN (DA1). Scale bars, 20 μm. Axes, D (dorsal), L (lateral).

Figure 3. Global gene expression dynamics of PNs.

(A) Visualization of PNs from 4 different developmental stages: 0h APF, 24h APF, 48h APF, and adult sequenced using either *VT033006-GAL4* or *GH146-GAL4*. tSNE dimensionality reduction was performed using 1216 genes identified by iterative clustering for identifying markers (ICIM) among them. **(B)** Hierarchical heatmap showing the expression of the top 52 out of 474 differentially expressed genes identified among PNs of different developmental stages. **(C)** Examples of the expression of the dynamic genes. Cells are colored according to the expression level of each gene. *Akap200* (A kinase anchor protein 200, encodes a scaffolding protein that contributes to the maintenance and regulation of cytoskeletal structure), *cib* (ciboulot, encodes an actin binding protein), and *fax* (failed axon connections, a gene involved in axon development) have the highest expression in early pupal stage and are downregulated gradually. *Rdl* (Resistant to dieldrin, encodes a chloride channel), *slo* (slowpoke, encodes a subunit of calcium-activated potassium channel), and *CG8177* (Anion exchanger 2), are upregulated as PNs develop. **(D, E)** Top 474 differentially expressed genes can be divided into 8 groups based on their dynamic profiles—2 groups without obvious developmental trend (not shown), 5 groups of down-regulated genes (D), and 2 groups of up-regulated genes (E). Pink lines represent individual genes and the black line shows mean expression of genes in each group. The highest expression is normalized as 1 for all genes. The top 10 GO terms for up-regulated and down-regulated genes are shown on right.

Figure 4. PN transcriptomes show distinct features at different stages of development.

(A) Visualization of most PNs from 0h APF, 24h APF, 48h APF, and adults using tSNE based on genes identified by ICIM at each stage. Adult clusters (circled) are identified using HDBSCAN. **(B)** Clustering of 0h APF PNs using HDBSCAN identified two clusters. **(C)** Part of the molecular pathways critical for neurite pruning in *Drosophila*. **(D)** Genes whose function have been implicated in neurite pruning have higher expression in cluster 0: *Sox14* (p-value: 5.01E-51), *Mical* (p-value: 1.49E-09), *Cul1* (p-value: 8.15E-4), *shrb* (p-value: 6.37E-19) and *Vps20* (p-value: 1.23E-17) (Mann-Whitney U test). **(E, F)**. PN transcriptomic similarity calculated at the cell level (mean inverse Euclidean distance calculated using 1216 ICIM genes identified from PNs of all 4 stages) and the cluster level (Pearson correlation calculated using differentially expressed genes identified from 24h PN clusters) for adPNs (E) [0h APF: 587 cells, cell-level similarity (mean ± standard deviation): 0.350 ± 0.036, 15 clusters, cluster-level

similarity (mean ± standard deviation): 0.615 ± 0.160; 24h APF: 547 cells, cell-level similarity: 0.292 ± 0.041, 15 clusters, cluster-level similarity: 0.395 ± 0.189; 48h APF: 301 cells, cell-level similarity: 0.377 ± 0.046, 13 clusters, cluster-level similarity: 0.484 ± 0.212; adult stage: 209 cells, cell-level similarity: 0.422 ± 0.058, 15 clusters, cluster-level similarity: 0.741 ± 0.129] and lPNs (F) [0h APF: 484 cells, cell-level similarity: 0.402 ± 0.052, 10 clusters, cluster-level similarity: 0.736 ± 0.129; 24h APF: 354 cells, cell-level similarity: 0.360 ± 0.056, 10 clusters, cluster-level similarity: 0.474 ± 0.057; 48h APF: 296 cells, cell-level similarity: 0.385 ± 0.043, 10 clusters, cluster-level similarity: 0.570 ± 0.171; adult stage: 191 cells, cell-level similarity: 0.444 ± 0.057, 8 clusters, cluster-level similarity: 0.754 ± 0.141)]. **(G)** Schematic summary of PN transcriptome similarity changes from early pupal stage to adulthood. PN diversity peaks during circuit assembly around 24h APF and gradually diminishes as they develop into mature neurons. **(H)** Expression of *VAChT*, *Gad1*, and *VGlut* in adult PNs.

Figure 4—figure supplement 1. Visualization of most PNs at different stages using tSNE.
Dimensionality reduction was computed using top 2000 overdispersed genes found at each stage.

Figure 4—figure supplement 2. Embryonically born and larval born PNs at 0h APF.
(A) The larger cluster at 0h APF consists of both adPNs (*acj6+*) and lPNs (*vvl+*) while the smaller cluster contains only adPNs. **(B)** Two types of embryonically born PNs, DA4l and VA6 PNs, are both mapped to the smaller cluster (details in Figure 7).

Figure 5. PN type identification by MARS.
(A) Dimensionality reduction of most PNs at 4 developmental stages by 561 ICIM genes found at 24h APF. **(B)** PN types identified by MARS. Different MARS clusters are illustrated in different colors.

Figure 5—figure supplement 1. PN type identification using two other independent methods.
(A) Dimensionality reduction by 24h ICIM genes followed by cluster identification using HDBSCAN. Circled cells belong to two PN types but are assigned to the same cluster using HDBSCAN. **(B)** Cluster identification by Leiden based on neighborhood graph computed on 24h ICIM genes. Circled cells belong to two PN types but are assigned to the same cluster using Leiden. **(C)** 24h APF PNs colored according to PN types validated in Figure 2. **(D)** PN types identified using MARS (same as Figure 5B). Some PN types which are incorrectly annotated by HDBSCAN or Leiden are correctly annotated as distinct clusters by MARS.

Figure 6. Two complementary approaches to match transcriptomic clusters representing same PN types at different developmental stages.
(A) scRNA-seq was performed for *kn+* PNs from 3 different developmental stages: 24h APF, 48h APF, and adult. **(B)** tSNE plots showing *kn+* PNs from three different stages, plotted separately. Cells are clustered according to 24h ICIM genes. Cell numbers are indicated. **(C)** *kn+* PNs from three different stages plotted in the same tSNE plot. Cells are clustered according to 24h ICIM genes. **(D)** Two approaches were used for matching the same PN types at different stages: 1) automatic prediction by calculating the transcriptomic similarity between clusters at two stages 2) manual matching of clusters using specific markers or marker combinations. **(E)** Jaccard similarity index of automatically matched transcriptomic clusters from different stages. Clusters #7 (brown cells in panel G) in 24h and 48h APF do not match with any cluster in the

adult stage; therefore, the similarity calculation is left as not applicable (NA). **(F)** Examples of markers used to manually match transcriptomic clusters representing the same PN types across different stages. **(G)** All *kn+* PN types (6 adPNs and 3 vPNs) are matched from three different stages. Two independent approaches (automatic and manual) produced similar results.

Figure 6—figure supplement 1. *kn+* adPN transcriptomes become more similar as development proceeds.

(A) Bar plot of Euclidean distance between all pairs of *kn+* cells using ICIM genes identified among them. *kn+* vPNs are excluded from this analysis. 24h APF: 98 cells, mean ± standard deviation: 0.374 ± 0.066; 48h APF: 174 cells, mean ± standard deviation (std): 0.446 ± 0.912; adult: 124 cells, mean ± std: 0.493 ± 0.085 **(B)** Bar plot of Pearson's correlation between all pairs of *kn+* adPN clusters. 24h APF: 6 clusters, mean ± std: 0.167 ± 0.141; 48h APF: 6 clusters, mean ± std: 0.424 ± 0.170; adult: 6 clusters, mean ± std: 0.506 ± 0.187.

Figure 7. Matching transcriptomic cluster representing the same PN types across four developmental stages.

(A) Visualization of most PNs at 4 different developmental stages: 0h APF, 24h APF, 48h APF, and adult. 561 ICIM genes at 24h APF PNs were used for dimensionality reduction. **(B)** Visualization of the same types of PNs at all developmental stages. Clusters with the same color represent same neuronal type. Light grey dots indicate cells that have neither been decoded nor matched. **(C)** Summary of transcriptomic clusters mapped to known PN types at different developmental stages. Solid red-lines indicate clusters we can unambiguously match using marker combinations; dashed red-lines indicate PN types we can narrow down to less than 3 transcriptomic clusters. Solid green-lines indicate clusters that are two-way matched automatically (two clusters from two stages are the most similar to each other); dashed green-lines indicates clusters that are one-way matched automatically (one cluster is the most similar with the other but not the other way around). Circles with white "+" indicate PN types that have been sequenced and confirmed at that stage using additional GAL4 lines (see Figure 7—figure supplement 1).

Figure 7—figure supplement 1. Supporting evidence for matching PN types across developmental stages.

(A, C) Visualization of *GH146+* PNs (grey) with *Mz19+* PNs (green) at 48h APF (A) and at the adult stage (C). PN type of *Mz19+* PNs shown on left were decoded previously (Li et al. 2017). **(B, D)** Visualization of *kn+* PNs from cells sequenced using *GH146-GAL4* (in grey) and cells sequenced using *kn-GAL4* (in blue) at 48h APF (A) and at the adult stage (C). Annotation of *kn-GAL4+* cells was done in Figure 6. **(E)** Visualization of the same types of PNs matched automatically (left) or manually (right) in tSNE space (same as Figure 7C). Transcriptomic clusters representing the same PN types of different developmental stages are labeled in the same color. Colors used to indicate PN types are identical to those in Figure 7B.

Figure 7—figure supplement 2. Markers used for manually matching PNs.

Dot plot of markers used to match the same types of PNs across different stages. Size of the dot represents percentage of cells expressing a given marker in a cluster at a given stage, and color of the dot represents expression level.

Figure 8. PN types with adjacent birth order share more similar transcriptomes at early pupal stages.
(A) Different PN types born from a common neuroblast follow a stereotyped sequence. The birth order of PNs determines to which glomerulus their dendrites target. The birth order of adPNs are shown on right. PN types with known transcriptomic identities at any of the four stages are highlighted in red. **(B)** Correlation matrix of the transcriptomes of adPNs with known identities (Pearson's correlation). PN types are ordered according to their birth order. At 0h and 24h APF, PN types with birth orders adjacent to each other exhibit the highest correlations in their transcriptomes, as indicated by high correlations in boxes just off the diagonal line. **(C)** Results of permutation test under the null hypothesis that the ranks of adPN transcriptomic similarity do no covary with the ranks of birth order. Observed values is the average Spearman correlation of 8 adPN types decoded in all 4 stages (red dot). The distribution is the average Spearman correlations obtained by randomly permutating the birth order for 5000 iterations (histogram). **(D)** Developmental trajectory analysis showing an unbiased pseudo time of 0h APF adPNs (embryonically born types excluded). The pseudo time roughly matches their birth order. **(E)** Expression levels of 15 genes in adPNs with known identity at 0h APF. These genes have been shown to exhibit temporal expression gradient in PN neuroblasts (Liu et al. 2015). The highest expression is normalized as 1 for all genes.

Figure 8—figure supplement 1. Hierarchical clustering of all excitatory PNs.
Hierarchical clustering of all excitatory PN clusters of 0h APF **(A)**, 24h APF **(B)**, 48h APF **(C)**, and adult **(D)**. Correlation calculation and hierarchical clustering were based on the principal components calculated using the entire gene matrix. adPNs are indicated by green bar and lPNs are indicated by orange bar on the top and left side of each plot. Clusters that have been matched to specific PN types are labeled.

Figure 9. Differentially expressed genes between different PN types.
(A) Number of differentially expressed (DE) genes identified at each developmental stage among all excitatory PN clusters or among the 12 PN types that are matched in all four stages. 103 and 52 genes are differentially expressed in all four stages among all excitatory PN types or among the 12 PN types, respectively. **(B)** Percentage of transcription factors (TFs) or cell-surface molecules (CSMs) from the list of genes that are differentially expressed among PNs in all four stages compared to the genome-wide percentage. **(C, D)** Dot plot of the 17 TFs (C) and 23 CSMs (D) that are differentially expressed in all four stages among the 12 PN types.

Figure 9—figure supplement 1
Dot plot of 114 TFs that are differentially expressed in any of the four stages among the 12 PN type matched across all stages.

Figure 9—figure supplement 2
Dot plot of 228 CSMs that are differentially expressed in any of the four stages among the 12 PN type matched across all stages.

Figure 10. Differentially expressed genes among different PN types in the adult stage.
(A) Venn diagram of differentially DE genes at 24h APF (497 genes) and in adults (542 genes). **(B)** Top 10 biological process terms of DE genes found in 24h APF PNs only (top), in both 24h APF and adults PNs (middle), and in adult PNs only (bottom). GO terms associated with neural

development are colored in orange, and GO terms associated with metabolism are colored in blue. **(C)** Dot plot of adult DE genes that belong to the ‘ion channels’ (top) or ‘transmembrane receptors’ (bottom) gene group from FlyBase. PN types are separated by lineage and decoded PN types are labeled and ordered according to their birth order within each lineage.

Figure 1

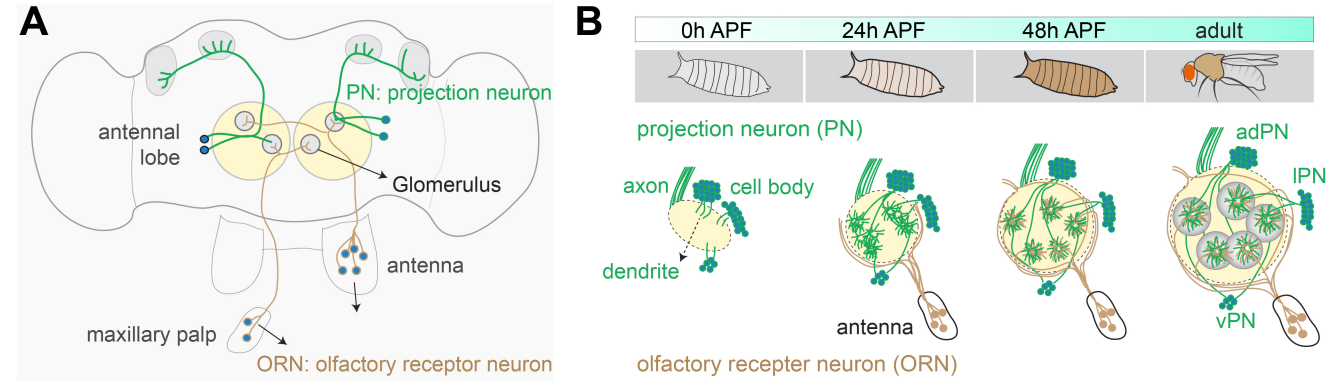

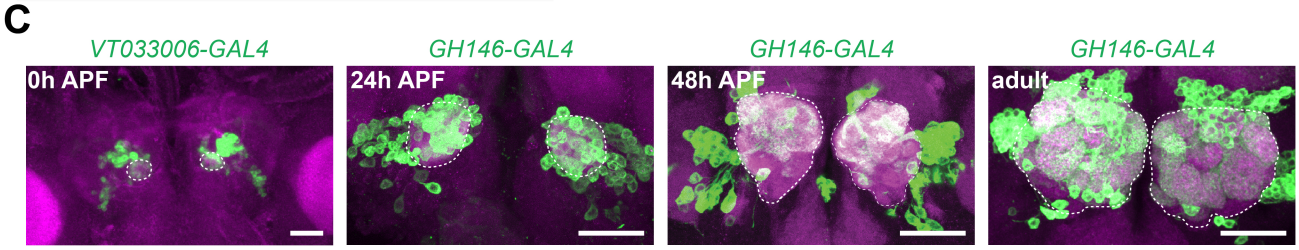

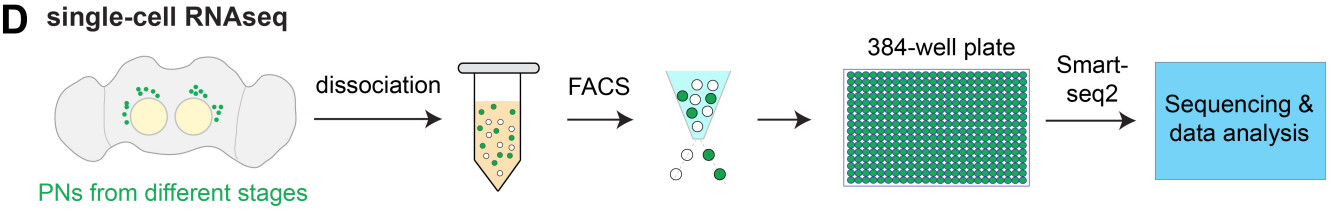

E

	0h	24h	48h	adult
most PN (~40 types)	1158	946	888	641
Mz19-GAL4 (3 types)		123	92	95
knot-GAL4 (8 types)		114	209	141
split#28-GAL4 (2 types)		104		
split#7-GAL4 (8 types)		334		
split#15-GAL4 (2 types)		89		
Total PNs	1158	1720	1189	877

Li et al., 2017 | newly sequenced

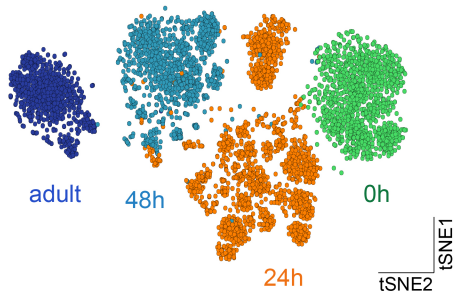

Figure 1 supplement 1

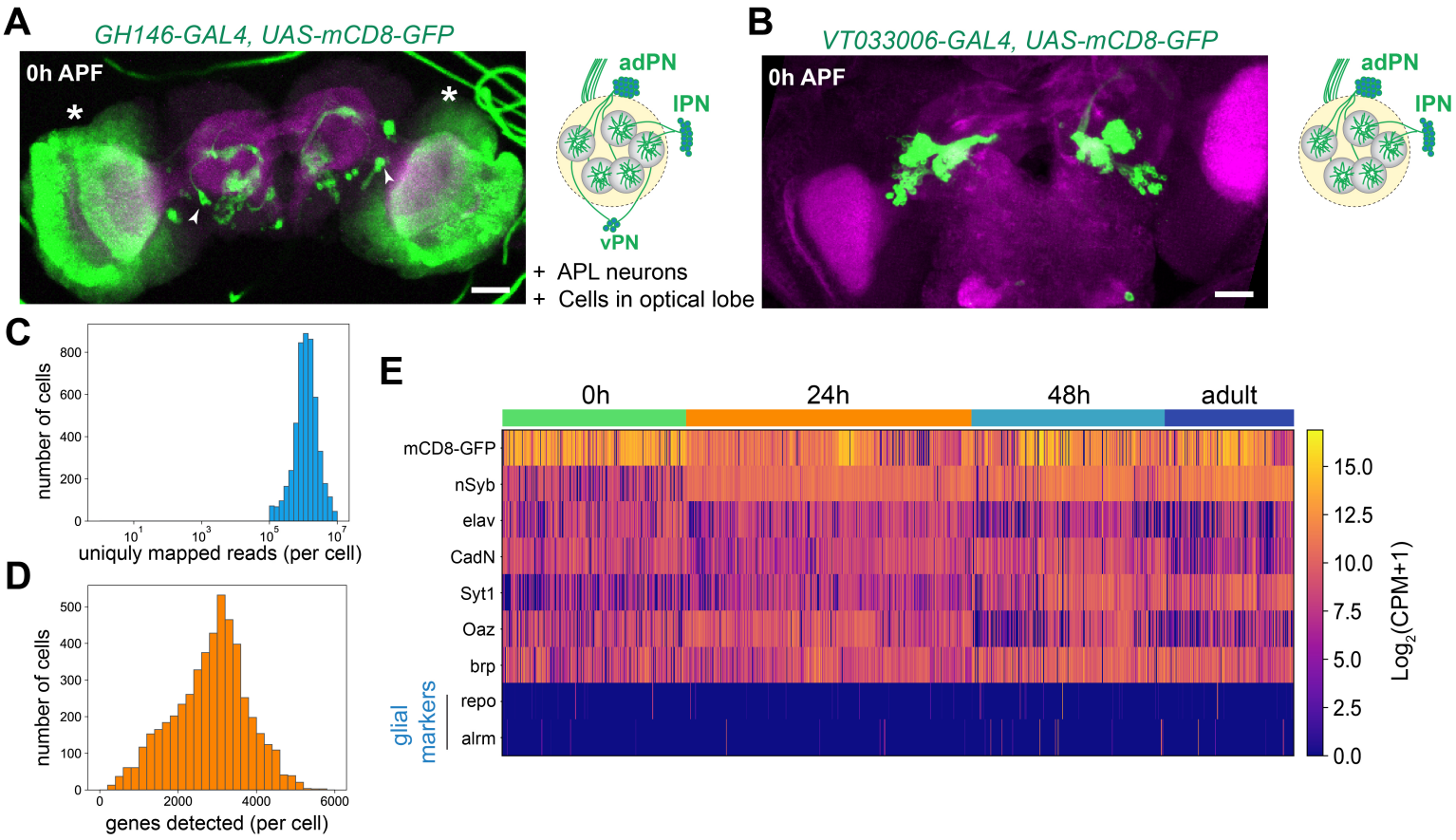

Figure 2

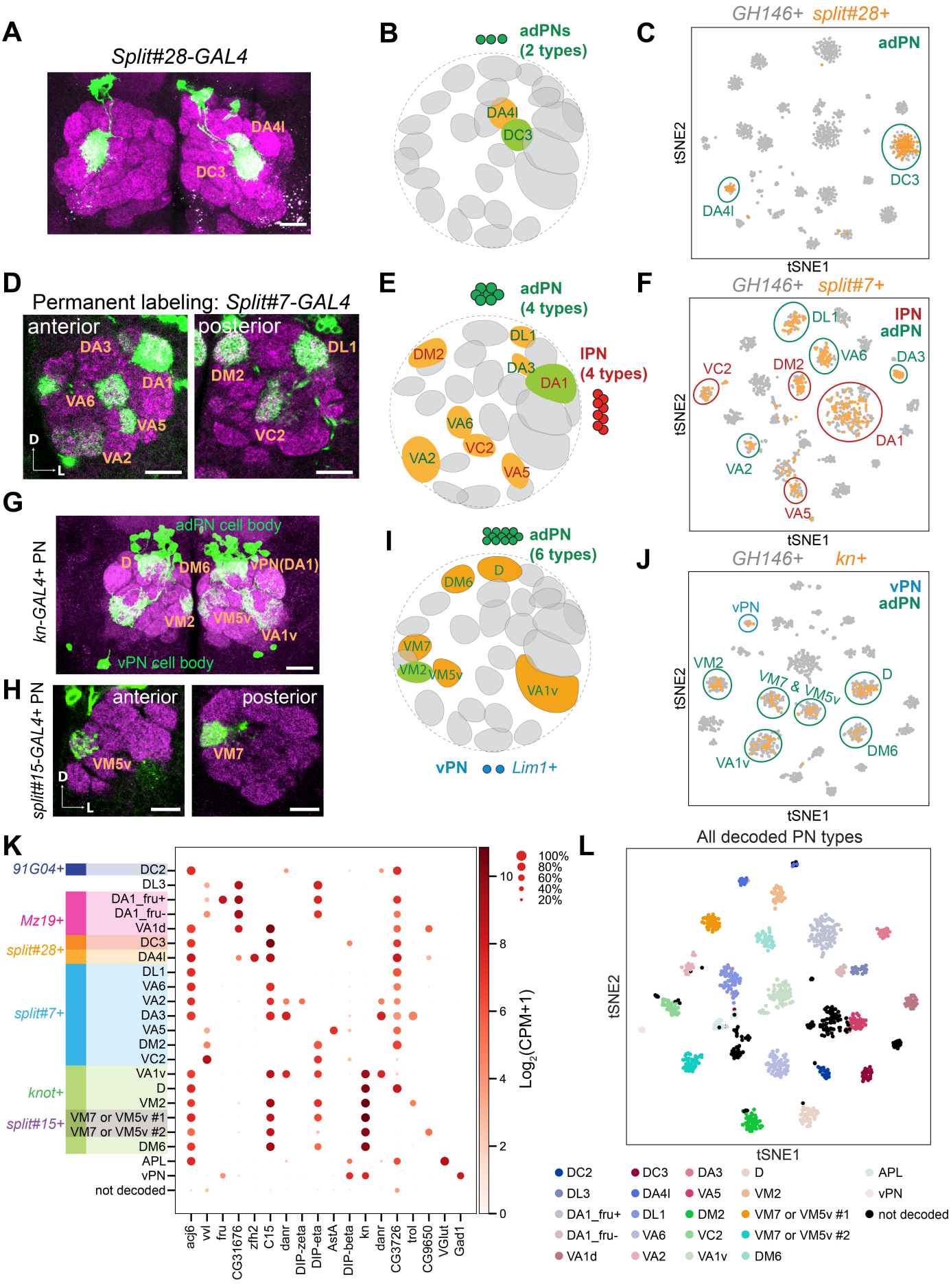
A
Split#28-GAL4
DA4l
DC3
B
adPNs
(2 types)
DA4l
DC3
C
GH146+ split#28+
adPN
DC3
DA4l
tSNE2
tSNE1
D
Permanent labeling: Split#7-GAL4
anterior
DA3
DA1
VA6
VA5
VA2
D
L
posterior
DL1
DM2
VC2
E
adPN
(4 types)
DL1
DM2
DA3
DA1
IPN
(4 types)
VA6
VC2
VA2
VA5
F
GH146+ split#7+
IPN
adPN
DL1
VA6
DA3
VC2
DM2
DA1
VA2
VA5
tSNE2
tSNE1
G
kn-GAL4+ PN
adPN cell body
D
DM6
vPN(DA1)
VM2
VM5v
VA1v
vPN cell body
H
split#15-GAL4+ PN
anterior
VM5v
D
L
posterior
VM7
I
adPN
(6 types)
D
DM6
VM7
VM2
VM5v
VA1v
vPN
Lim1+
J
GH146+ kn+
vPN
adPN
vPN
VM2
VM7 & VM5v
D
DM6
VA1v
tSNE2
tSNE1
K
91G04+
Mz19+
split#28+
split#7+
knot+
split#15+
DC2
DL3
DA1_fru+
DA1_fru-
VA1d
DC3
DA4l
DL1
VA6
VA2
DA3
VA5
DM2
VC2
VA1v
D
VM2
VM7 or VM5v #1
VM7 or VM5v #2
DM6
APL
vPN
not decoded
100%
80%
60%
40%
20%
Log2(CPM+1)
10
8
6
4
2
0
acj6
vvl
fru
CG31676
zfh2
C15
danr
DIP-zeta
DIP-eta
AstA
DIP-beta
kn
danr
CG3726
trol
CG9650
VGlut
Gad1
L
All decoded PN types
tSNE2
tSNE1
DC2
DC3
DA3
D
APL
DL3
DA4l
VA5
VM2
vPN
DA1_fru+
DL1
DM2
VM7 or VM5v #1
not decoded
DA1_fru-
VA6
VC2
VM7 or VM5v #2
VA1d
VA2
VA1v
DM6

Figure 2 supplement 1

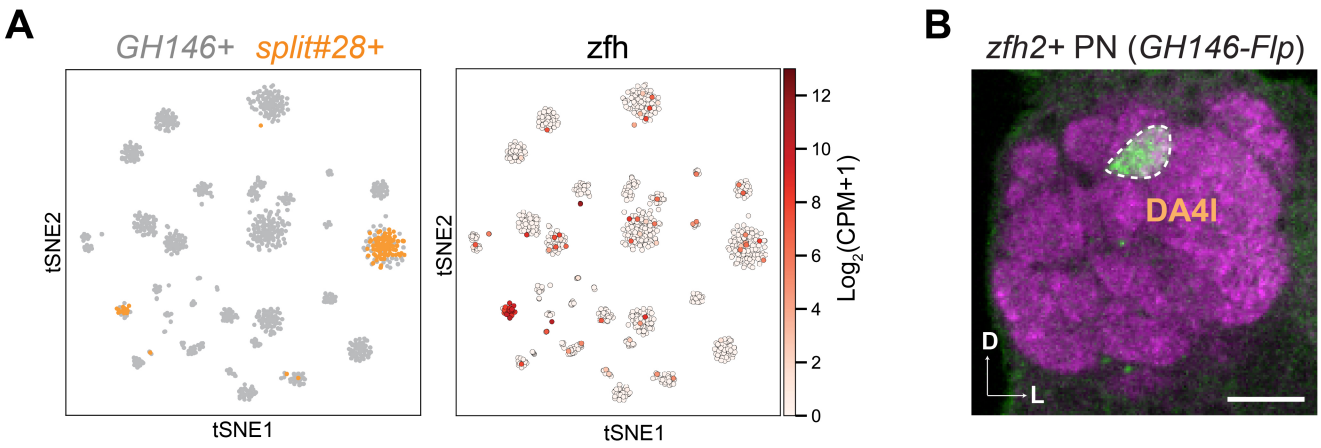

Figure 2 supplement 2

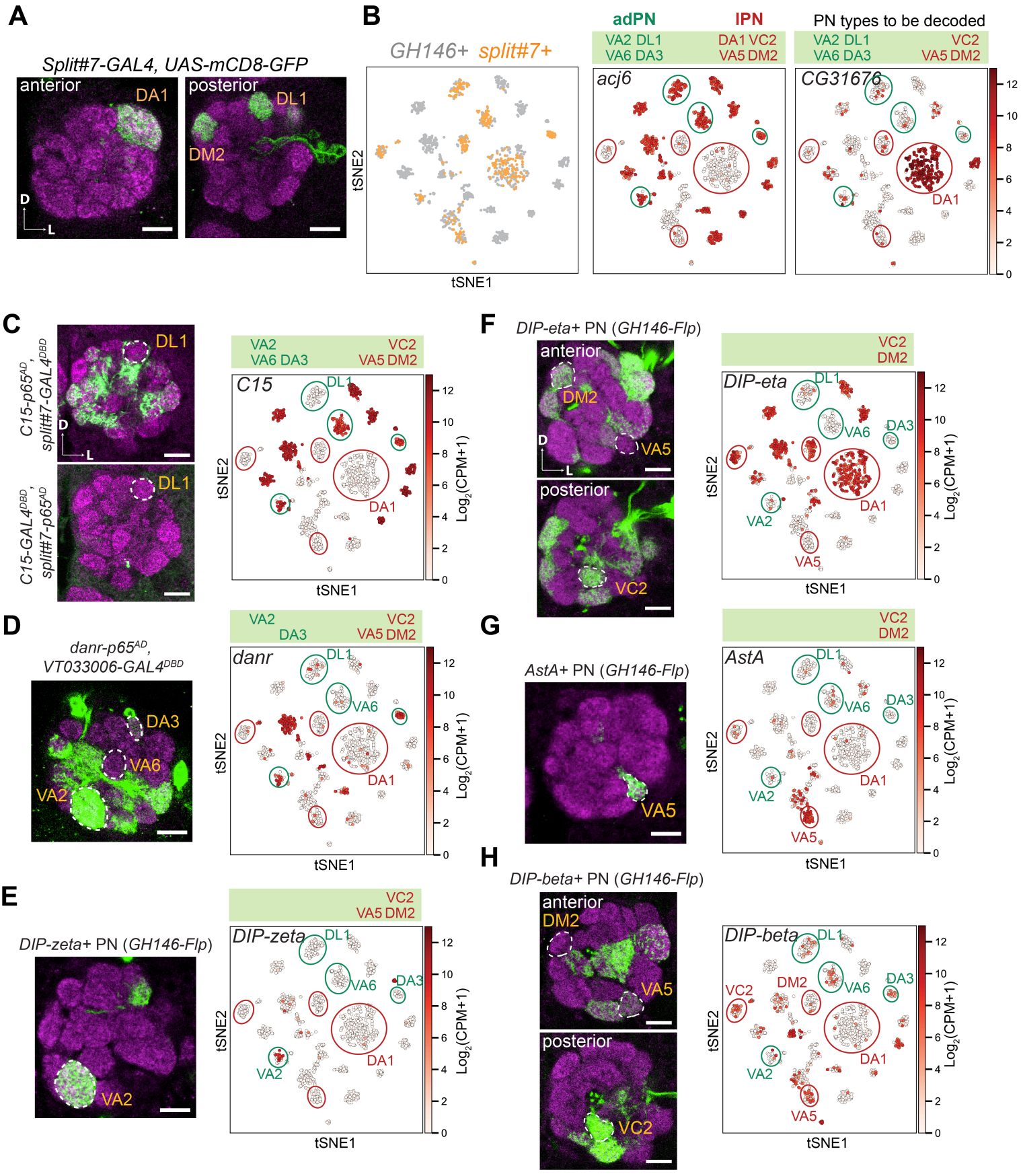

Figure 2 supplement 3

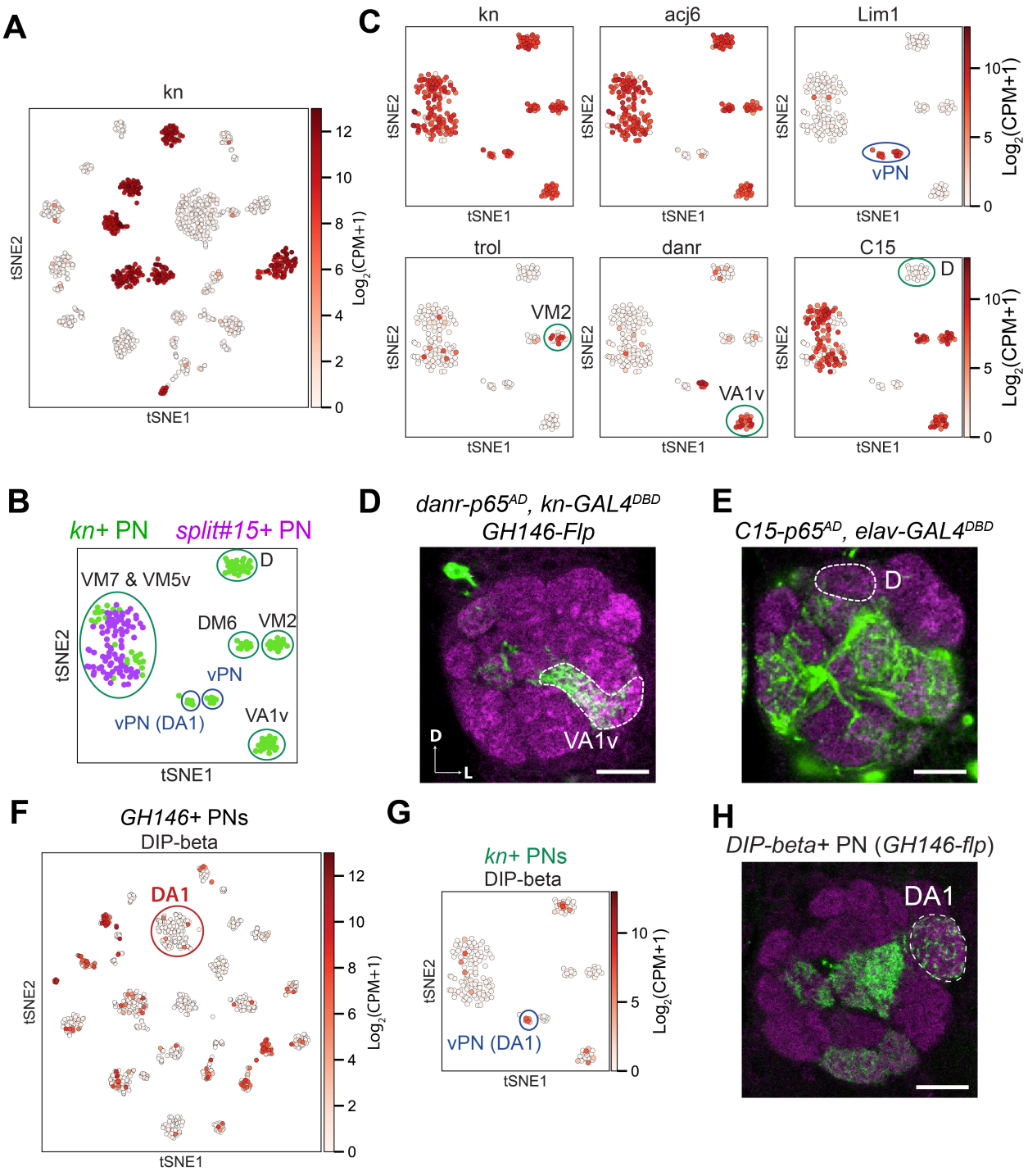

Figure 3

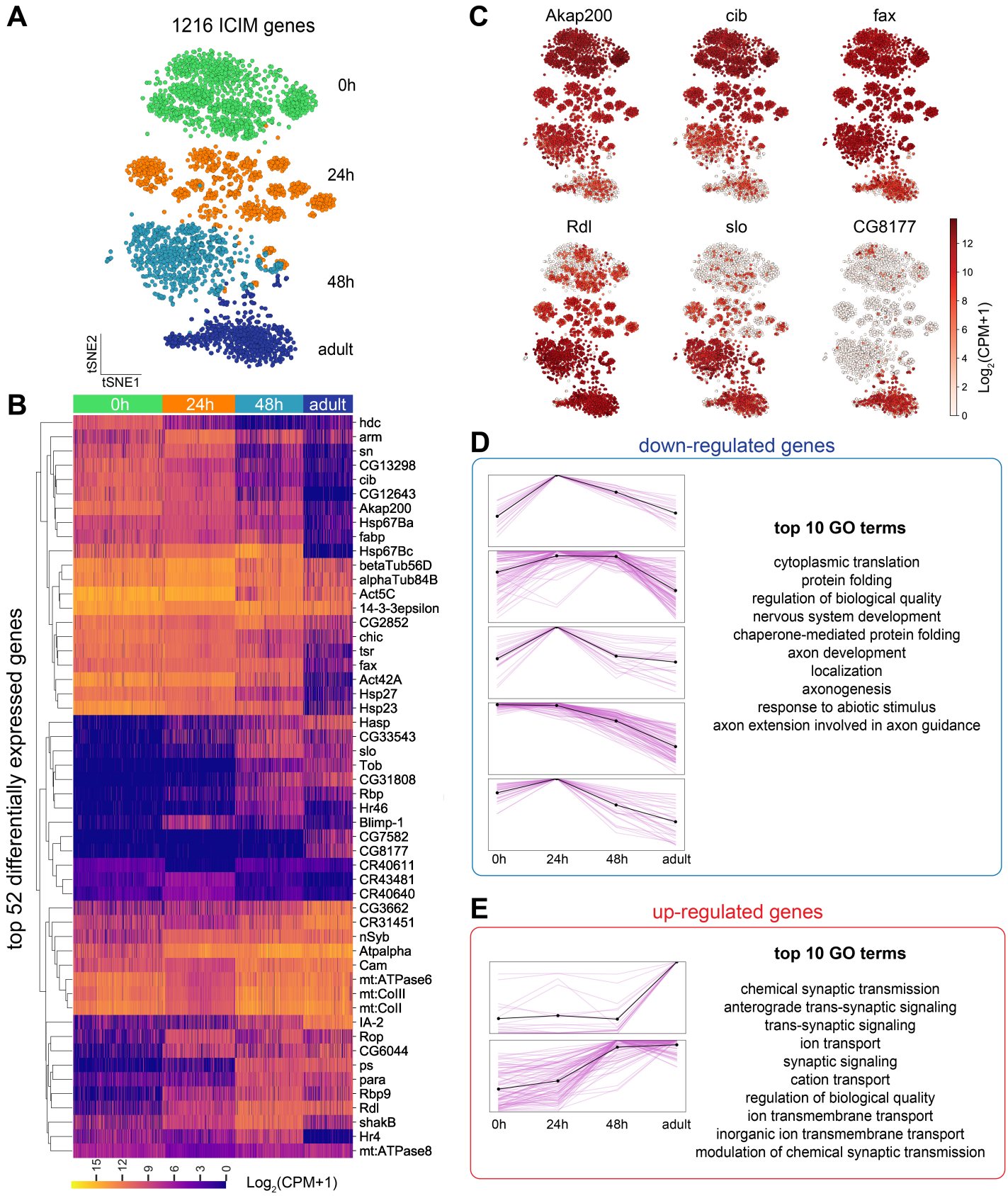
A
1216 ICIM genes
0h
24h
48h
adult
tSNE2
tSNE1
B
0h
24h
48h
adult
top 52 differentially expressed genes
hdc
arm
sn
CG13298
cib
CG12643
Akap200
Hsp67Ba
fabp
Hsp67Bc
betaTub56D
alphaTub84B
Act5C
14-3-3epsilon
CG2852
chic
tsr
fax
Act42A
Hsp27
Hsp23
Hasp
CG33543
slo
Tob
CG31808
Rbp
Hr46
Blimp-1
CG7582
CG8177
CR40611
CR43481
CR40640
CG3662
CR31451
nSyb
Atpalpha
Cam
mt:ATPase6
mt:CoIII
mt:CoI
IA-2
Rop
CG6044
ps
para
Rbp9
Rdl
shakB
Hr4
mt:ATPase8
15
12
9
6
3
0
Log2(CPM+1)
C
Akap200
cib
fax
Rdl
slo
CG8177
12
10
8
6
4
2
0
Log2(CPM+1)
D
down-regulated genes
0h
24h
48h
adult
top 10 GO terms
cytoplasmic translation
protein folding
regulation of biological quality
nervous system development
chaperone-mediated protein folding
axon development
localization
axonogenesis
response to abiotic stimulus
axon extension involved in axon guidance
E
up-regulated genes
0h
24h
48h
adult
top 10 GO terms
chemical synaptic transmission
anterograde trans-synaptic signaling
trans-synaptic signaling
ion transport
synaptic signaling
cation transport
regulation of biological quality
ion transmembrane transport
inorganic ion transmembrane transport
modulation of chemical synaptic transmission

Figure 4

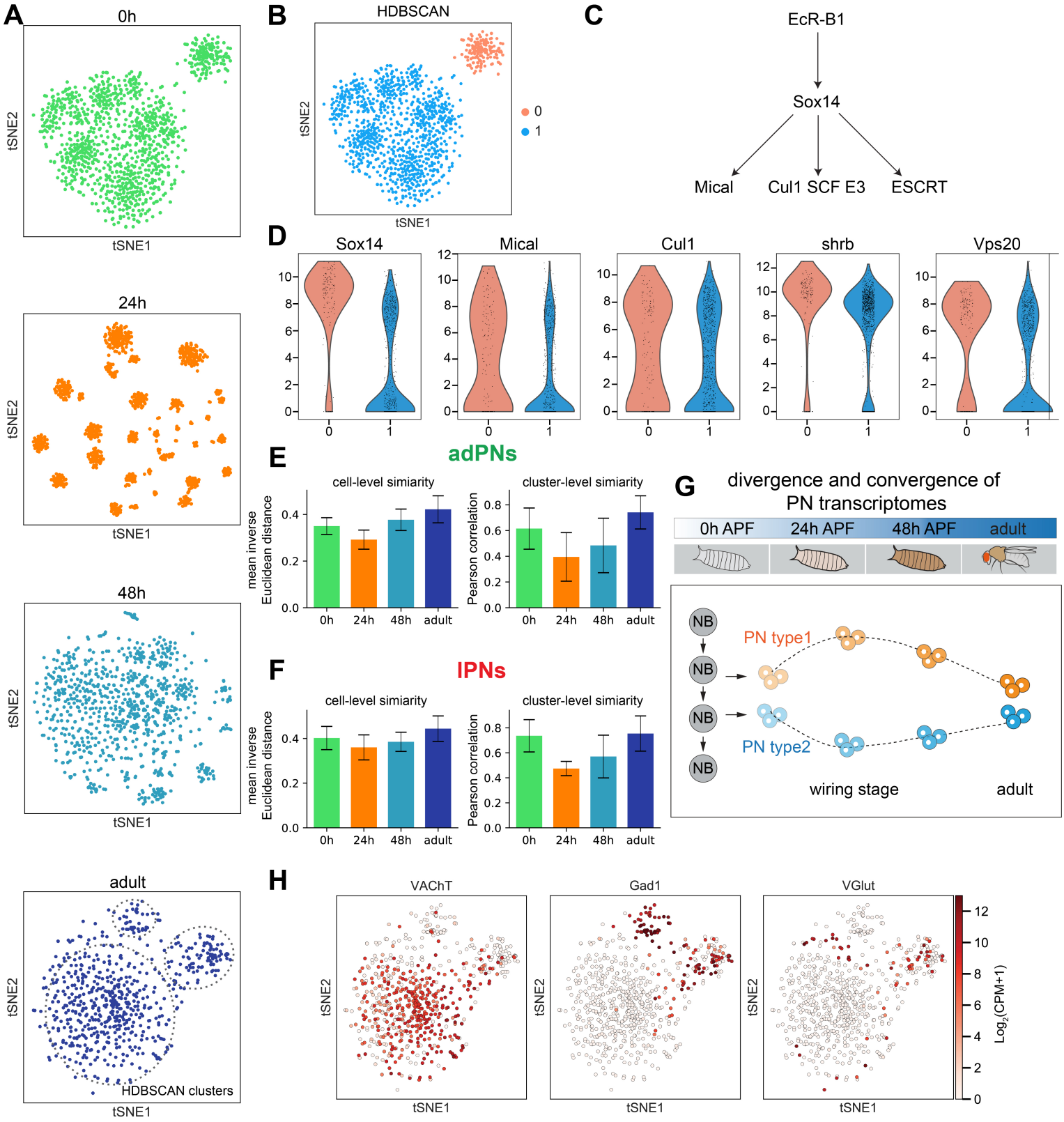
A
0h
24h
48h
adult
tSNE1
tSNE2
HDBSCAN clusters
B
HDBSCAN
0
1
C
EcR-B1
Sox14
Mical
Cul1 SCF E3
ESCRT
D
Sox14
Mical
Cul1
shrb
Vps20
E
adPNs
cell-level simiarity
cluster-level simiarity
mean inverse Euclidean distance
Pearson correlation
0h
24h
48h
adult
F
IPNs
G
divergence and convergence of PN transcriptomes
0h APF
24h APF
48h APF
adult
NB
PN type1
PN type2
wiring stage
H
VAChT
Gad1
VGlut
Log2(CPM+1)

Figure 4 supplement 1

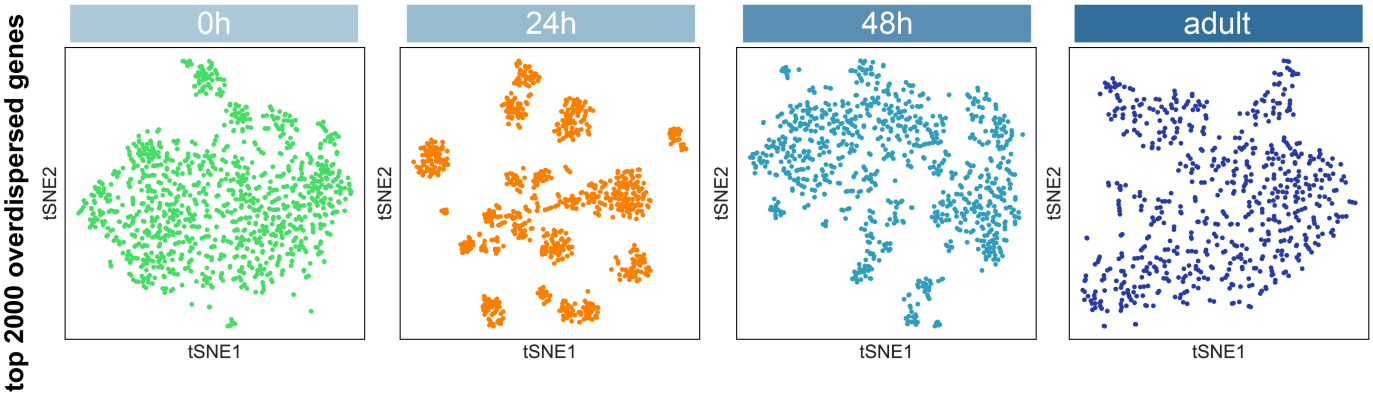

Figure 4 supplement 2

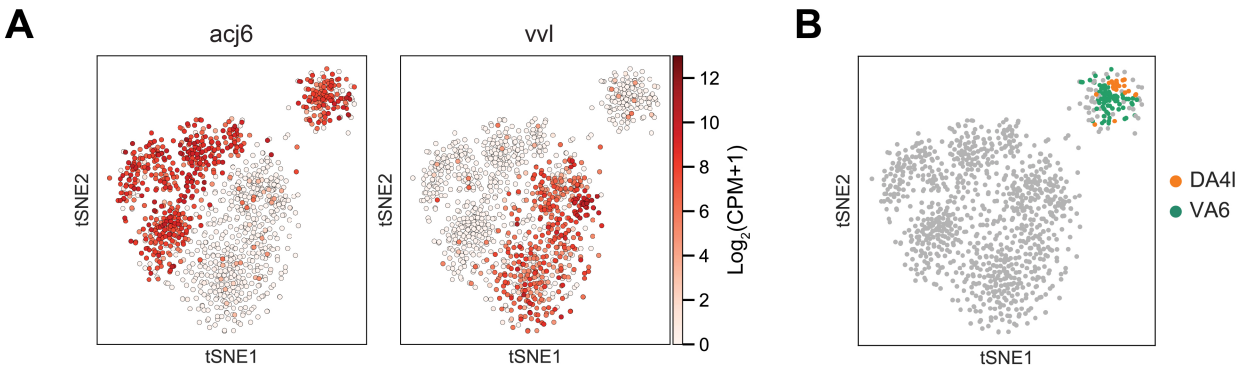

Figure 5

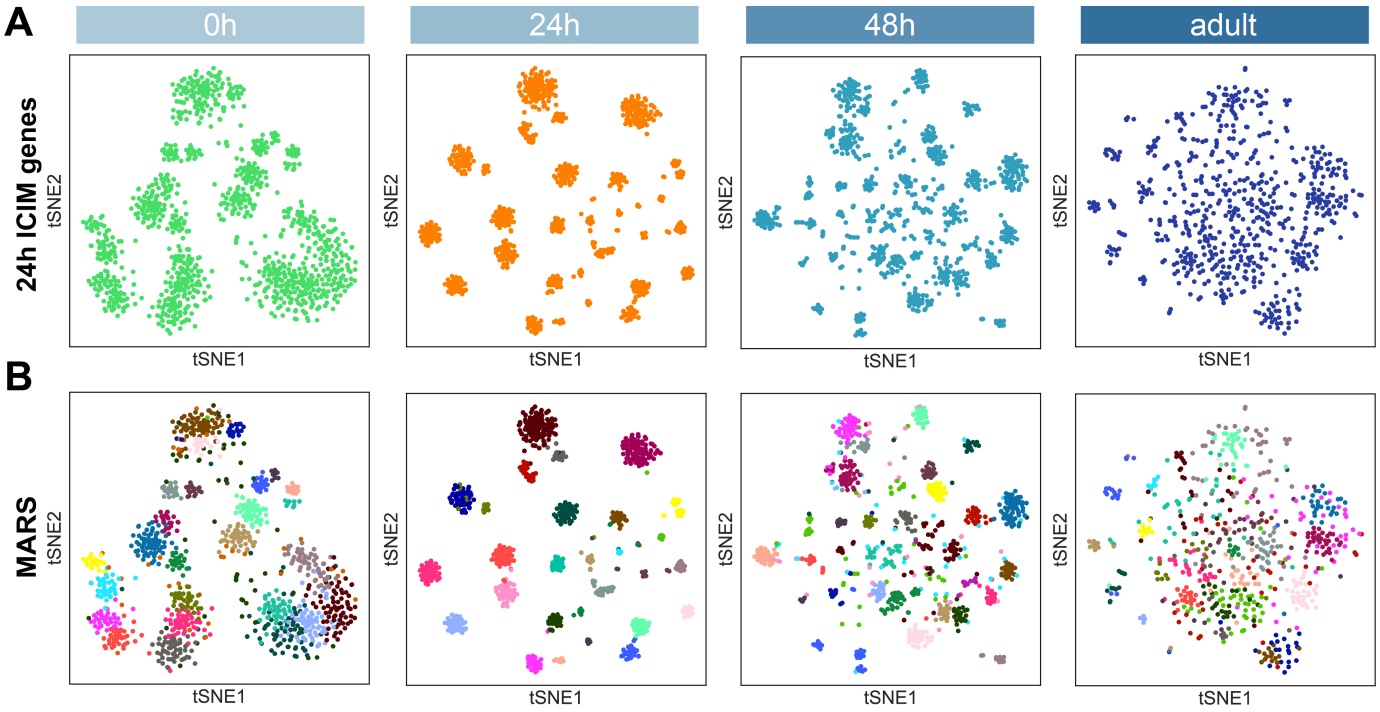
A
0h
24h
48h
adult
24h ICIM genes
tSNE2
tSNE1
B
MARS
tSNE2
tSNE1

Figure 5 supplement 1

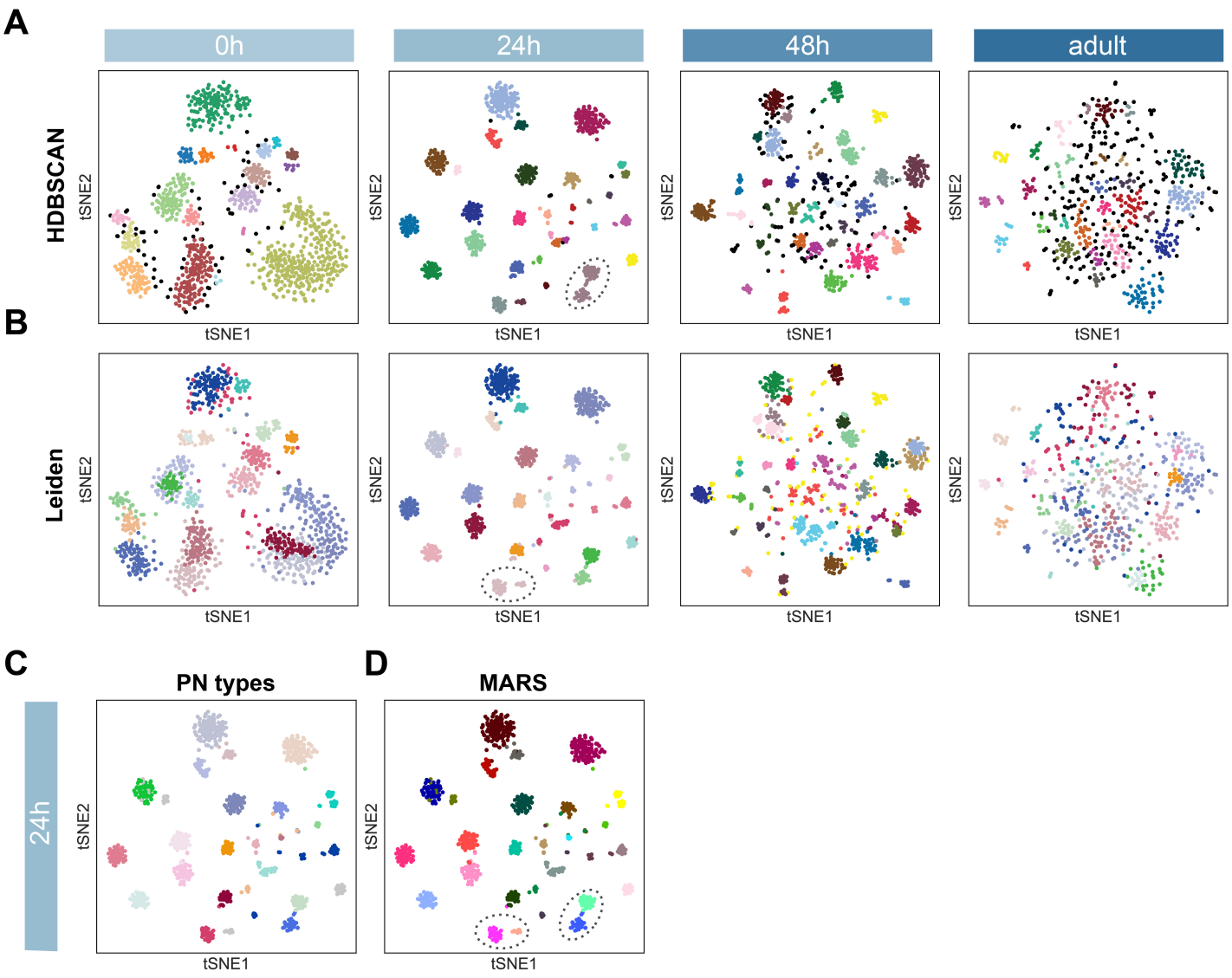

Figure 6

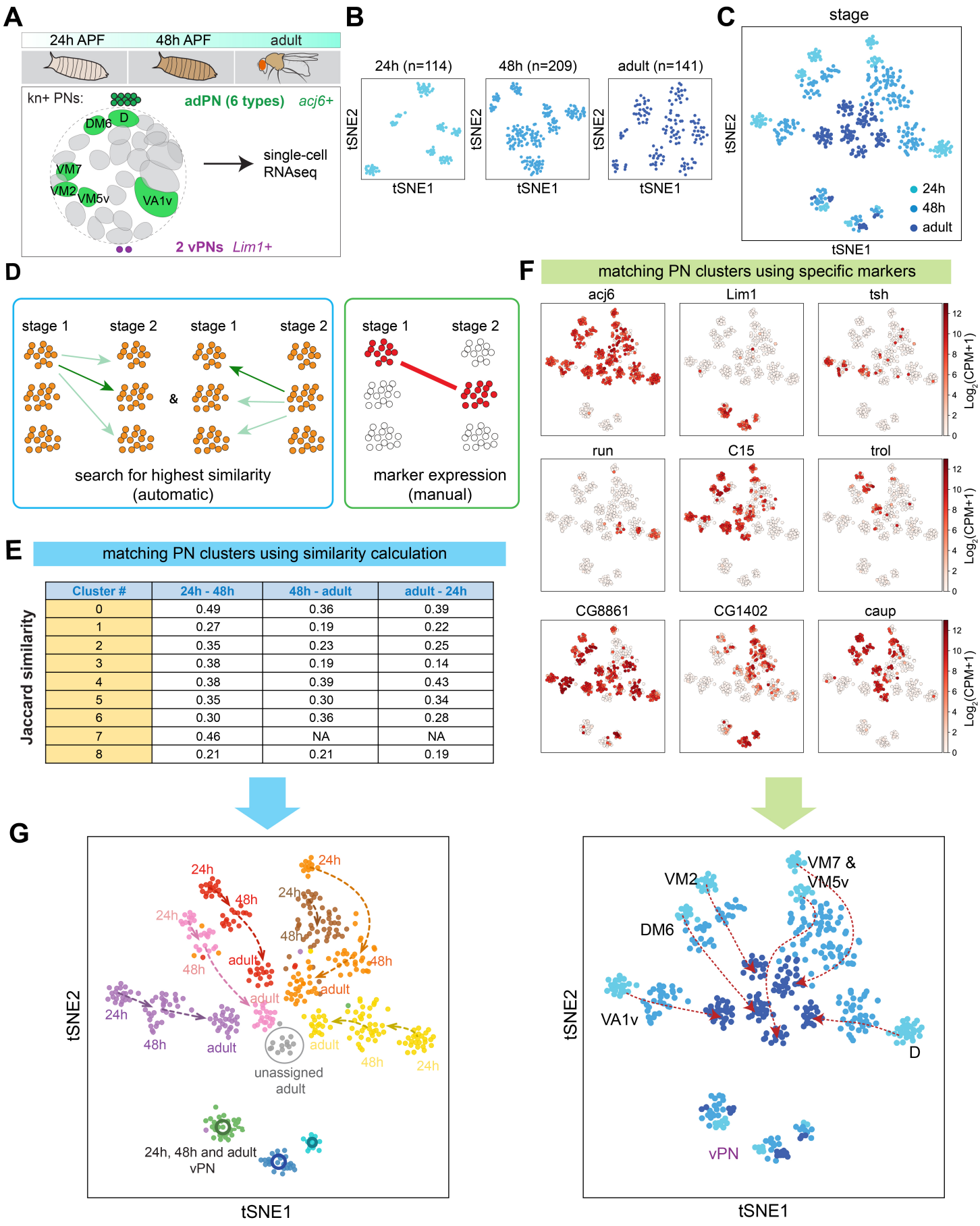

Cluster #	24h - 48h	48h - adult	adult - 24h
0	0.49	0.36	0.39
1	0.27	0.19	0.22
2	0.35	0.23	0.25
3	0.38	0.19	0.14
4	0.38	0.39	0.43
5	0.35	0.30	0.34
6	0.30	0.36	0.28
7	0.46	NA	NA
8	0.21	0.21	0.19

Figure 6 supplement 1

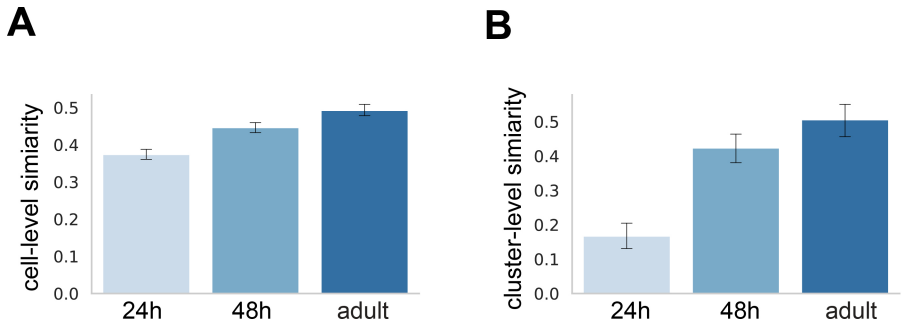

Figure 7

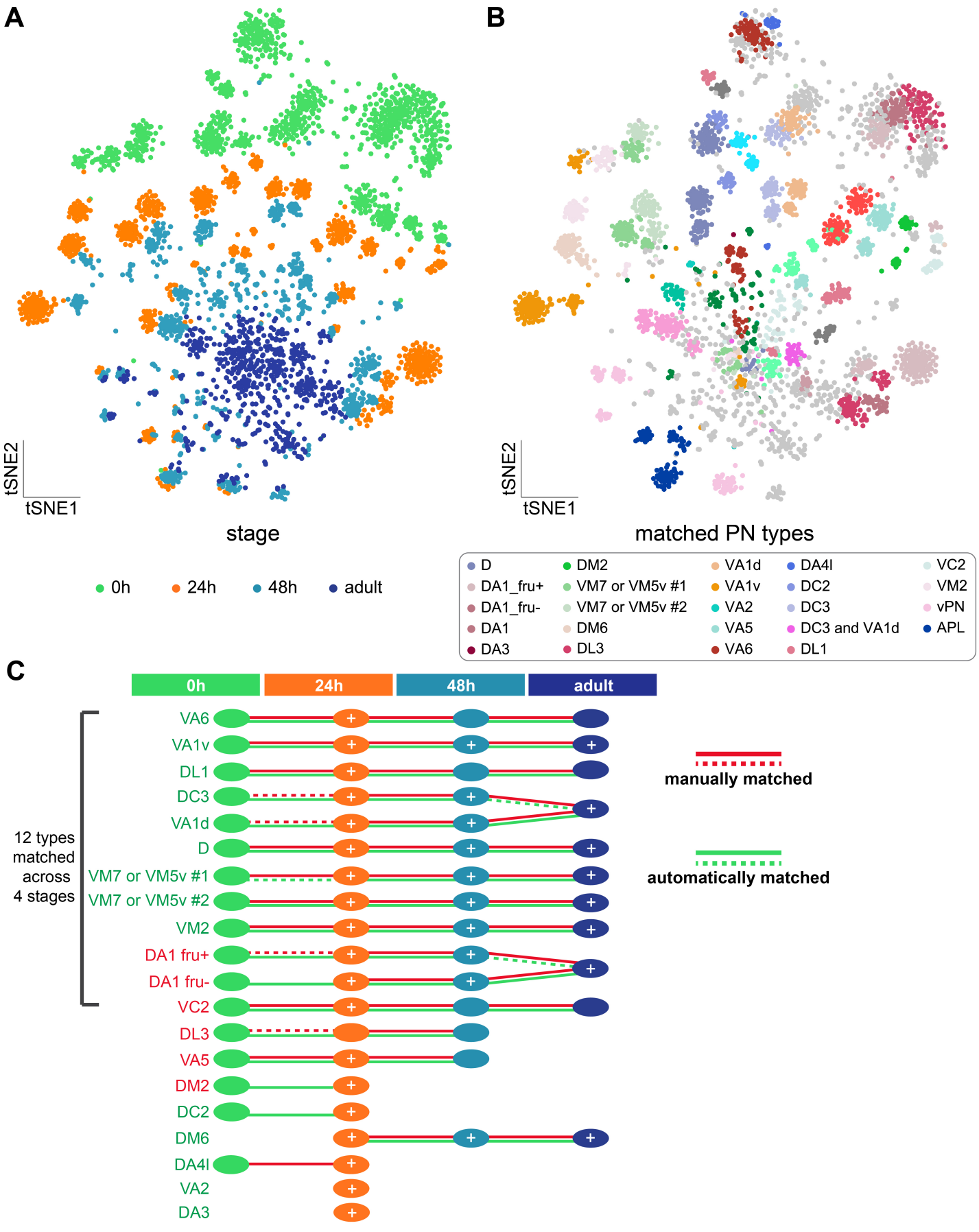
A
B
tSNE2
tSNE1
stage
0h
24h
48h
adult
matched PN types
D
DA1_fru+
DA1_fru-
DA1
DA3
DM2
VM7 or VM5v #1
VM7 or VM5v #2
DM6
DL3
VA1d
VA1v
VA2
VA5
VA6
DA4l
DC2
DC3
DC3 and VA1d
DL1
VC2
VM2
vPN
APL
C
0h
24h
48h
adult
VA6
VA1v
DL1
DC3
VA1d
D
VM7 or VM5v #1
VM7 or VM5v #2
VM2
DA1 fru+
DA1 fru-
VC2
DL3
VA5
DM2
DC2
DM6
DA4l
VA2
DA3
12 types matched across 4 stages
manually matched
automatically matched

Figure 7 supplement 1

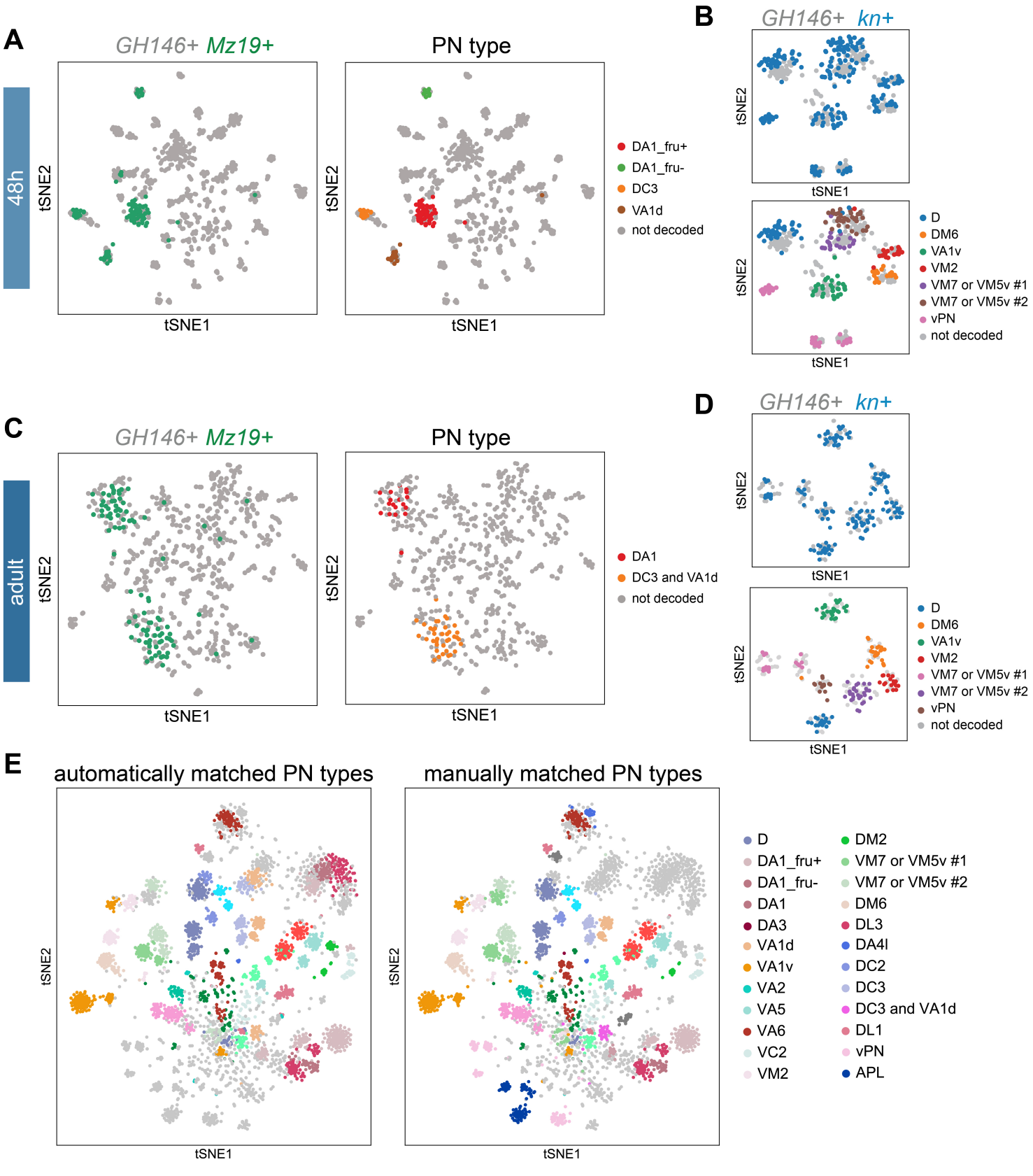

Figure 7 supplement 2

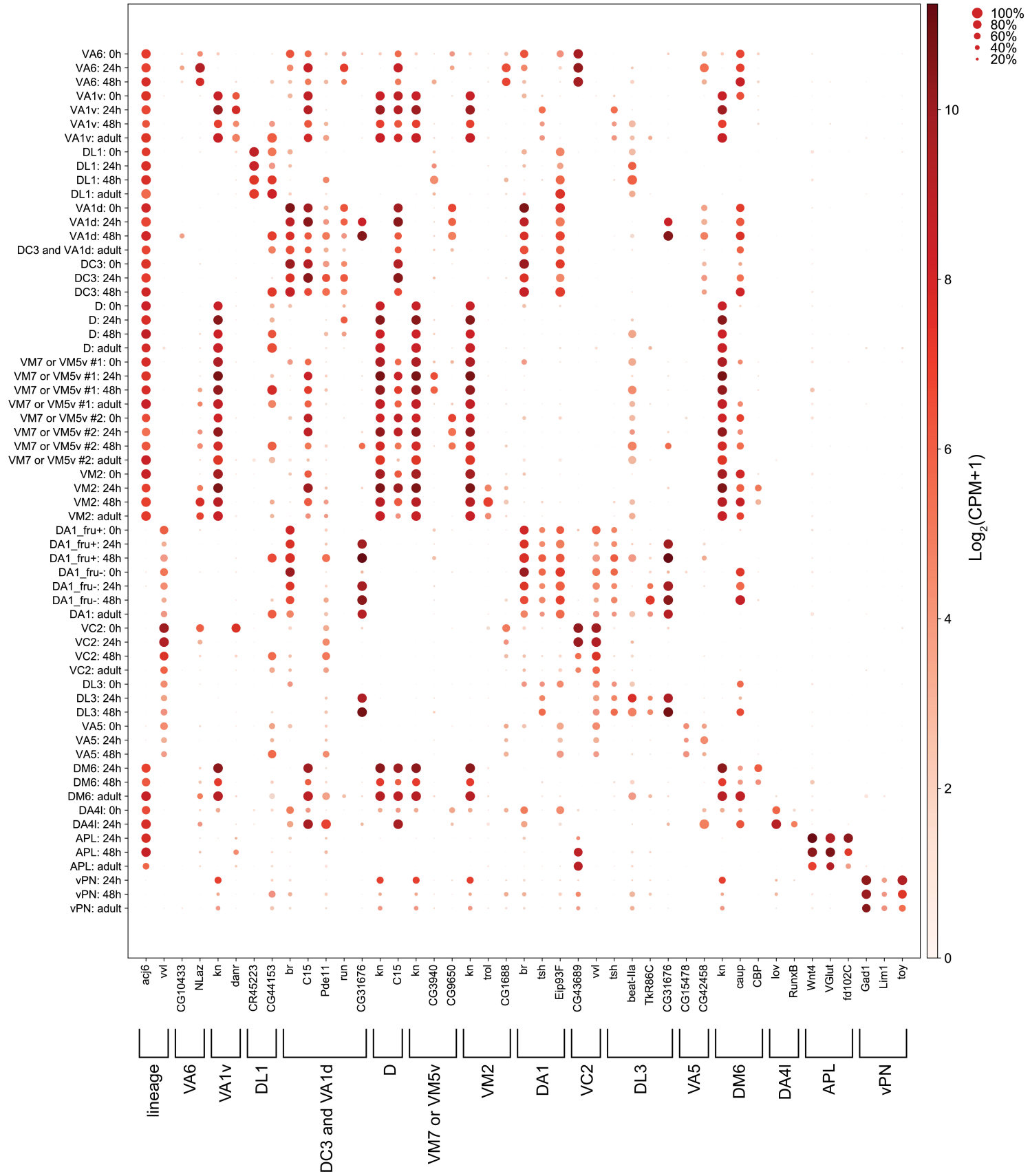

Figure 8

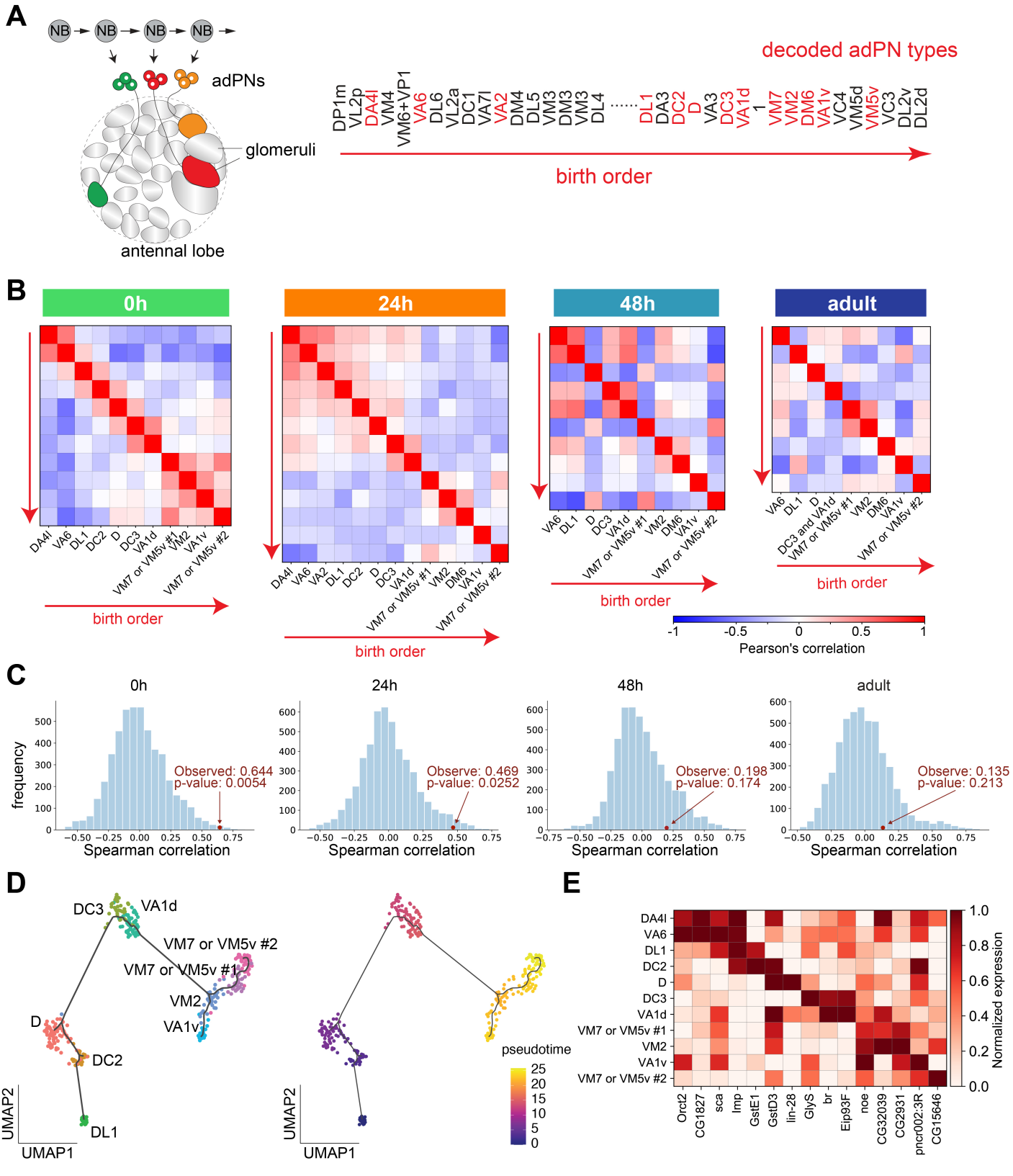
A
NB
adPNs
glomeruli
antennal lobe
decoded adPN types
DP1m VL2p DA4l VM4 VM6+VP1 VA6 DL6 VL2a DC1 VA7l VA2 DM4 DL5 VM3 DM3 VM3 DL4 ..... DL1 DA3 DC2 D VA3 DC3 VA1d 1 VM7 VM2 DM6 VA1v VC4 VM5d VM5v VC3 DL2v DL2d
birth order
B
0h
24h
48h
adult
DA4l VA6 DL1 DC2 D DC3 VA1d VM7 or VM5v #1 VM2 VA1v VM7 or VM5v #2
VA2 DM6
DC3 and VA1d
birth order
-1 -0.5 0 0.5 1
Pearson's correlation
C
0h
24h
48h
adult
frequency
Observed: 0.644
p-value: 0.0054
Observe: 0.469
p-value: 0.0252
Observe: 0.198
p-value: 0.174
Observe: 0.135
p-value: 0.213
Spearman correlation
D
DC3
VA1d
VM7 or VM5v #2
VM7 or VM5v #1
VM2
VA1v
D
DC2
DL1
UMAP2
UMAP1
pseudotime
25 20 15 10 5 0
E
DA4l VA6 DL1 DC2 D DC3 VA1d VM7 or VM5v #1 VM2 VA1v VM7 or VM5v #2
Orct2 CG1827 sca Imp GstE1 GstD3 lin-28 GlyS br Eip93F noe CG32039 CG2931 pncr002:3R CG15646
Normalized expression
1.0 0.8 0.6 0.4 0.2 0.0

Figure 8 supplement 1

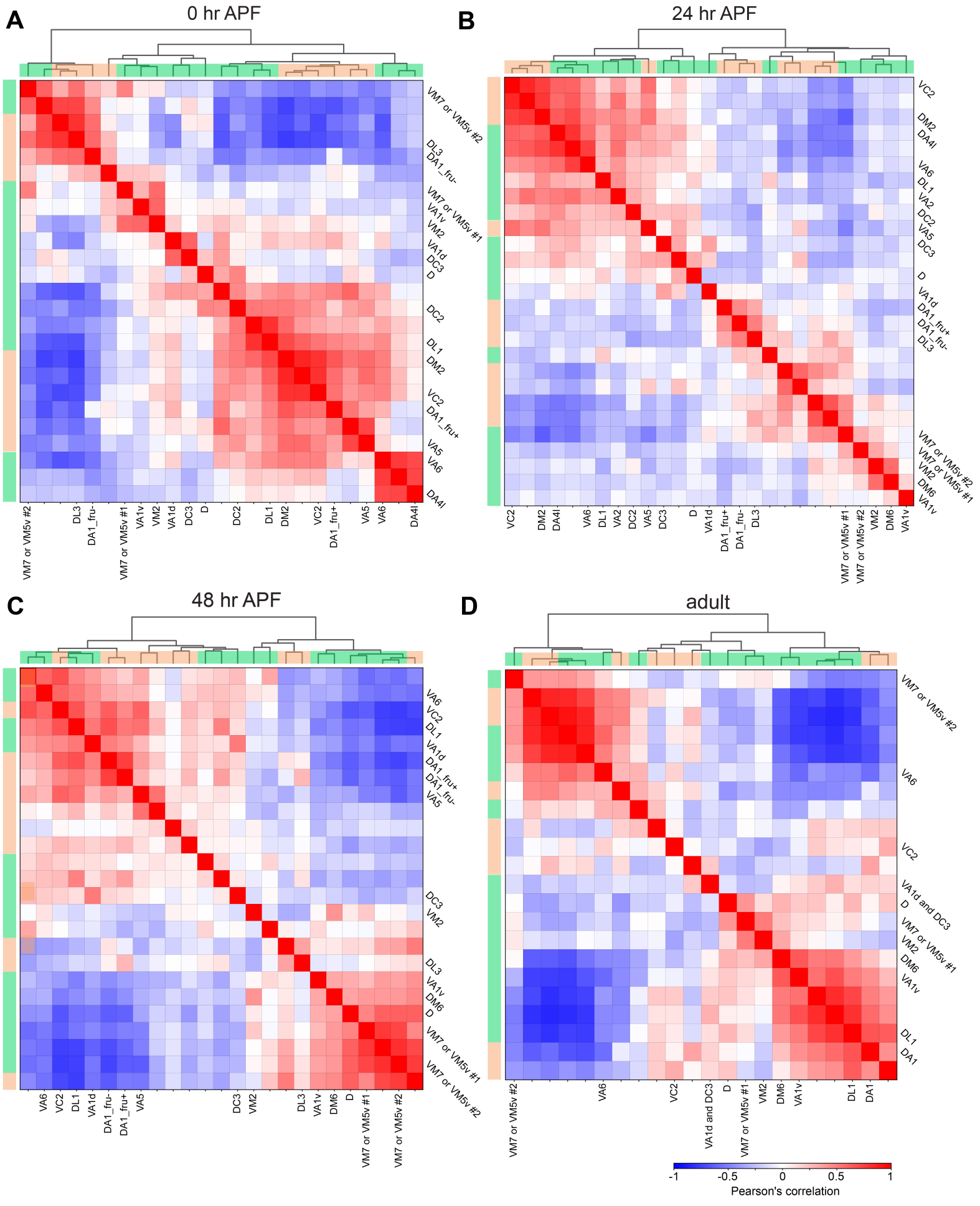

Figure 9

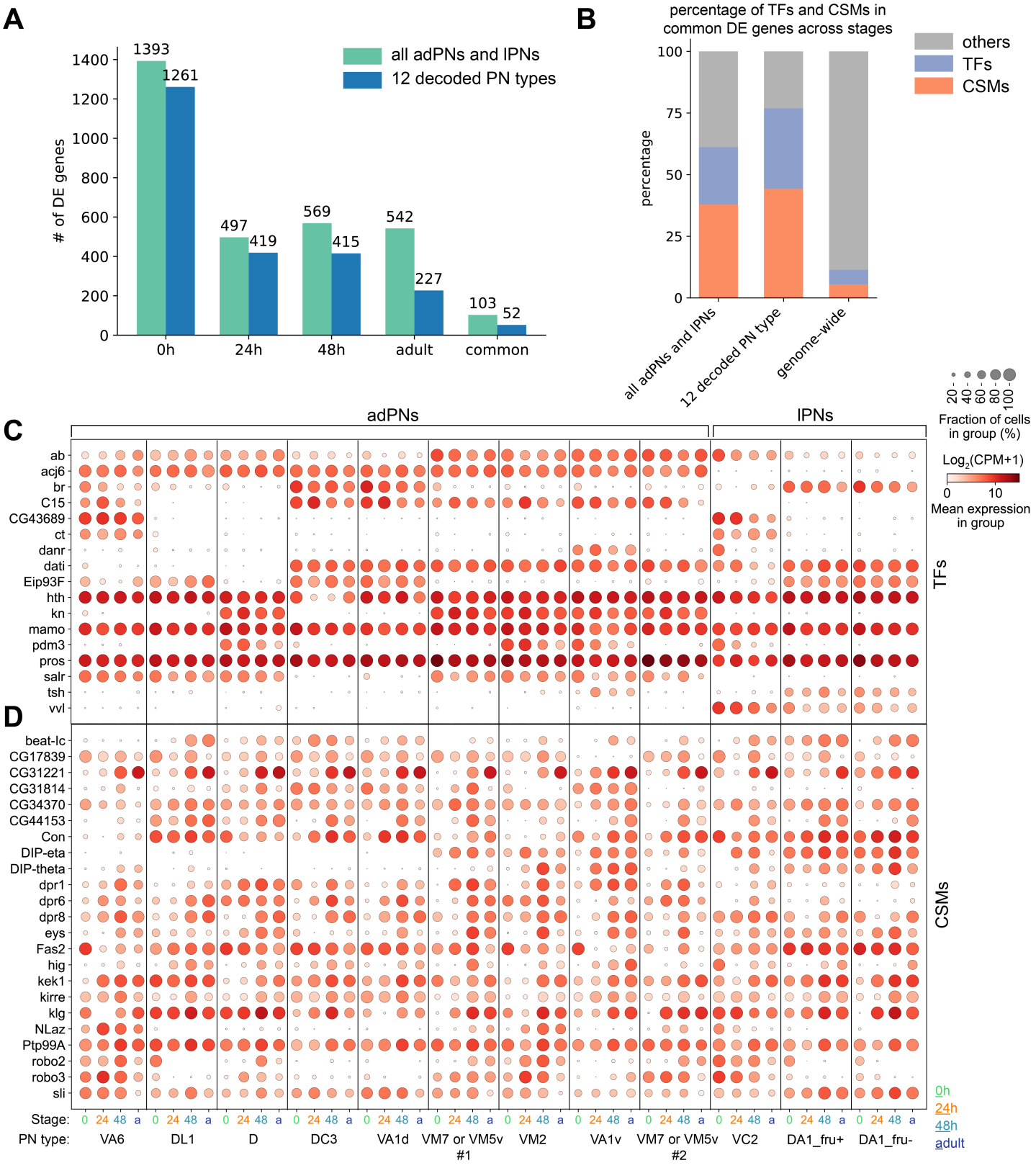
A
all adPNs and IPNs
12 decoded PN types
# of DE genes
1393
1261
497
419
569
415
542
227
103
52
0h
24h
48h
adult
common
B
percentage of TFs and CSMs in common DE genes across stages
others
TFs
CSMs
percentage
all adPNs and IPNs
12 decoded PN type
genome-wide
C
adPNs
lPNs
Fraction of cells in group (%)
Log2(CPM+1)
Mean expression in group
TFs
ab
acj6
br
C15
CG43689
ct
danr
dati
Eip93F
hth
kn
mamo
pdm3
pros
salr
tsh
vvl
D
CSMs
beat-Ic
CG17839
CG31221
CG31814
CG34370
CG44153
Con
DIP-eta
DIP-theta
dpr1
dpr6
dpr8
eys
Fas2
hig
kek1
kirre
klg
NLaz
Ptp99A
robo2
robo3
sli
Stage:
PN type:
VA6
DL1
D
DC3
VA1d
VM7 or VM5v #1
VM2
VA1v
VM7 or VM5v #2
VC2
DA1_fru+
DA1_fru-
0h
24h
48h
adult

Figure 9 Figure supplment 1

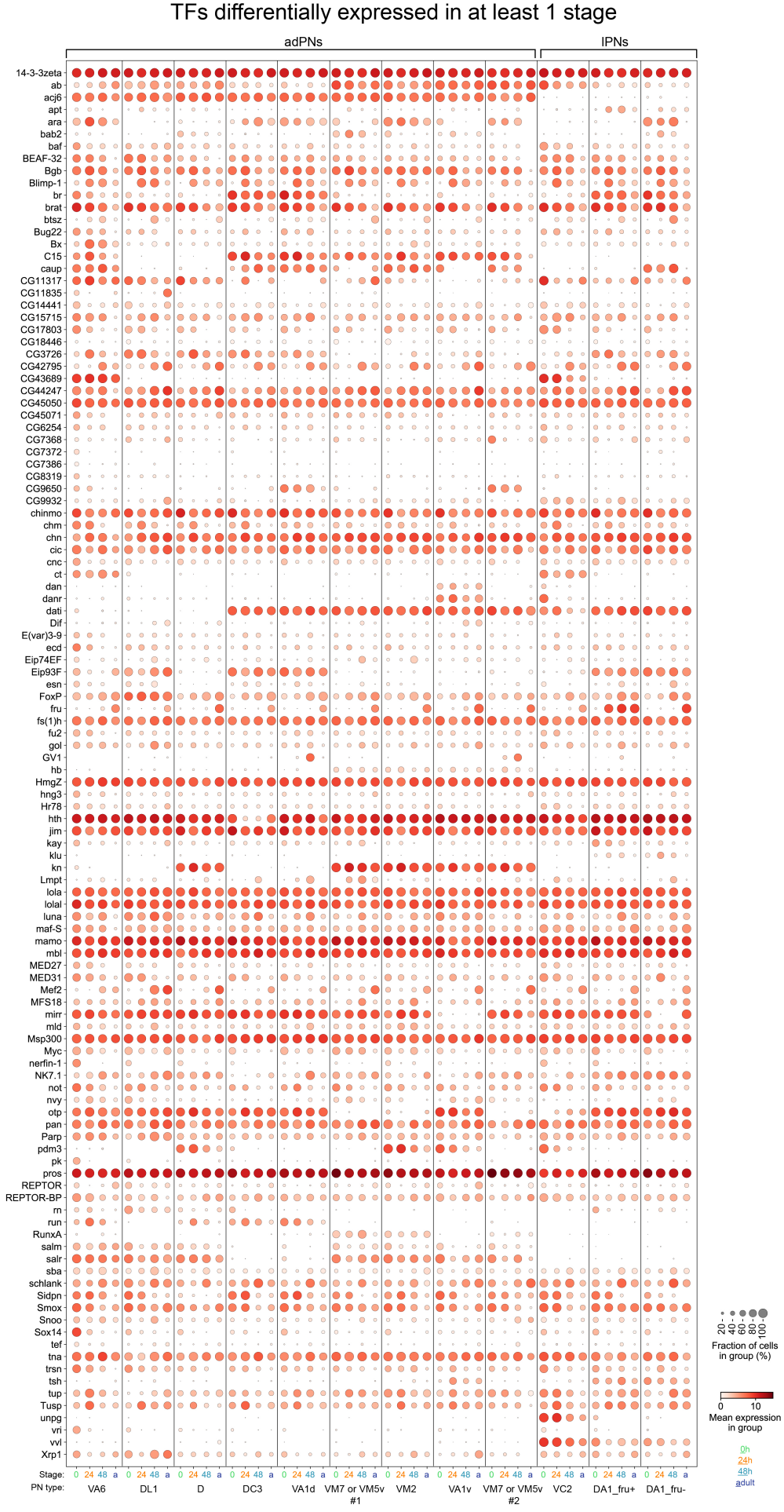

Figure 9 supplement 2

CSMs differentially expressed in at least 1 stage

Figure 10

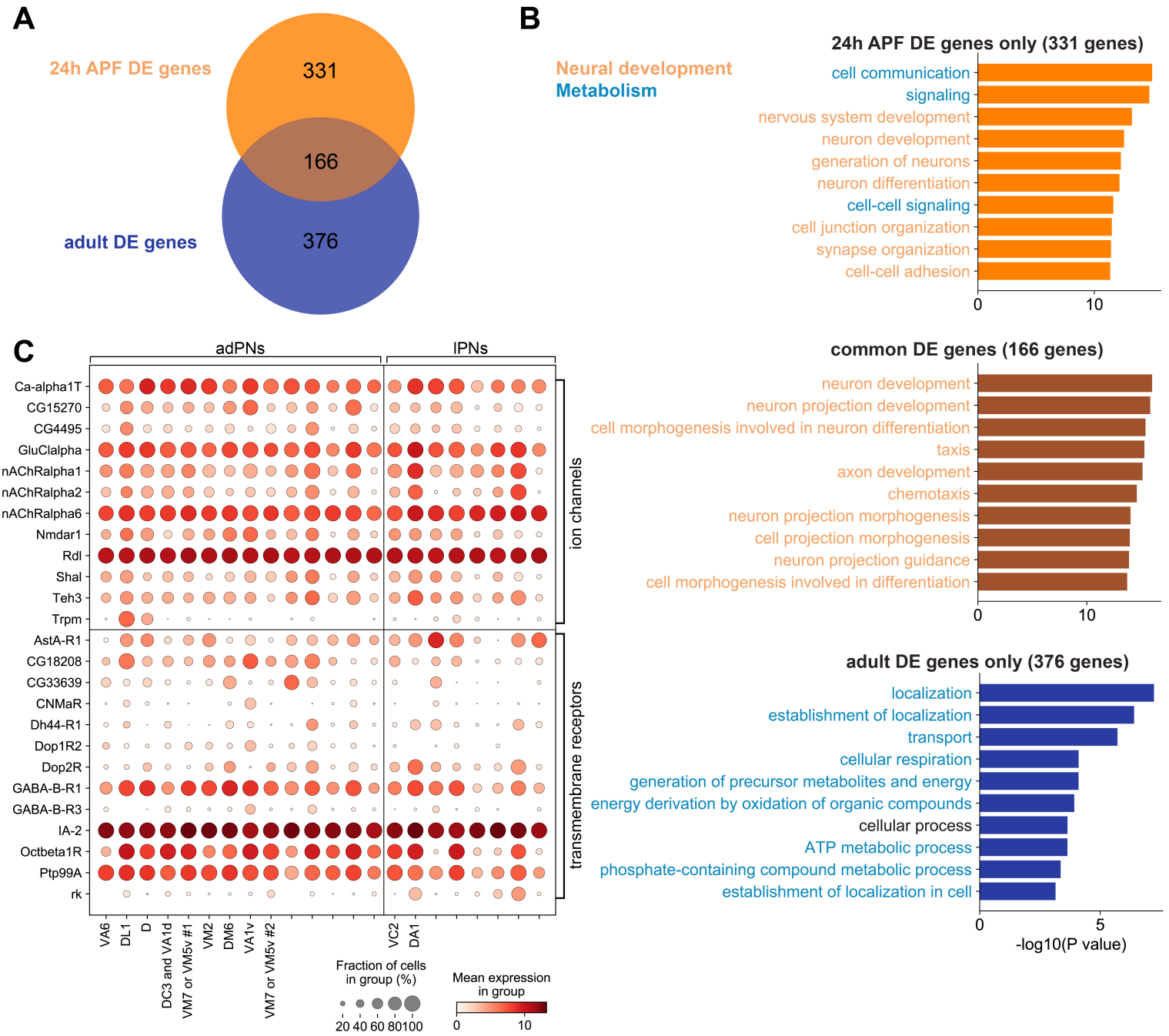
A
24h APF DE genes
331
166
adult DE genes
376
B
Neural development
Metabolism
24h APF DE genes only (331 genes)
cell communication
signaling
nervous system development
neuron development
generation of neurons
neuron differentiation
cell-cell signaling
cell junction organization
synapse organization
cell-cell adhesion
0
10
C
adPNs
lPNs
Ca-alpha1T
CG15270
CG4495
GluClalpha
nAChRalpha1
nAChRalpha2
nAChRalpha6
Nmdar1
Rdl
Shal
Teh3
Trpm
AstA-R1
CG18208
CG33639
CNMaR
Dh44-R1
Dop1R2
Dop2R
GABA-B-R1
GABA-B-R3
IA-2
Octbeta1R
Ptp99A
rk
ion channels
transmembrane receptors
VA6
DL1
D
DC3 and VA1d
VM7 or VM5v #1
VM2
DM6
VA1v
VM7 or VM5v #2
VC2
DA1
Fraction of cells in group (%)
20 40 60 80100
Mean expression in group
0
10
common DE genes (166 genes)
neuron development
neuron projection development
cell morphogenesis involved in neuron differentiation
taxis
axon development
chemotaxis
neuron projection morphogenesis
cell projection morphogenesis
neuron projection guidance
cell morphogenesis involved in differentiation
0
10
adult DE genes only (376 genes)
localization
establishment of localization
transport
cellular respiration
generation of precursor metabolites and energy
energy derivation by oxidation of organic compounds
cellular process
ATP metabolic process
phosphate-containing compound metabolic process
establishment of localization in cell
0
5
-log10(P value)